Throughput Maximization for Backscatter Communication in Cell-Free Symbiotic Radio Networks with Hybrid CSR-PSR

Kechen Zheng, *Senior Member, IEEE*, Zefu Li, Xiaoying Liu, *Senior Member, IEEE*, Jia Liu, *Senior Member, IEEE*, Tarik Taleb, *Senior Member, IEEE*, and Norio Shiratori, *Life Fellow, IEEE*

***Abstract*—With the evolution of sixth generation (6G) technologies and Internet of Things (IoT), base stations and IoT devices are deployed densely to achieve the ultra-high data rate, resulting in the scarcity of spectrum resource. To tackle it, we study a cell-free symbiotic radio network (CF-SRN) that consists of the cell-free network (CFN) and IoT network, and includes multiple access points (APs), multiple backscatter devices (BDs), and a single receiver. APs collaboratively transmit primary radio frequency (RF) signals to the receiver, and BDs split the energy of primary RF signals to perform backscatter communication, and energy harvesting. Existing works focus on the SRN with commensal symbiotic radio (CSR) or parasitic symbiotic radio (PSR) setup, while we design a hybrid CSR-PSR setup to balance the tradeoff between primary communication and backscatter communication in the CF-SRN. Based on the design, we formulate the sum backscatter throughput maximization problem by optimizing the time allocation vector, beamforming vectors of APs and BDs, and reflection coefficients of BDs, subject to the minimum sum primary throughput constraint. Due to the coupling relationship among high-dimensional variables, we decompose the formulated problem into time allocation optimization (TAO) subproblem, beamforming optimization (BO) subproblem, and reflection coefficient optimization (RCO) subproblem. For TAO subproblem, we use a linear programming method to obtain the optimal solution. For BO subproblem and RCO subproblem, we propose a block coordinate descent-based semi-definite relaxation and successive convex approximation (BSS) algorithm. Simulation results validate the superiority of the BSS algorithm and hybrid CSR-PSR setup.**

***Index Terms*—Symbiotic radio (SR), cell-free (CF), beamforming, throughput maximization.**

I. Introduction

With the emergence of ultra-high-definition video and telemedicine applications, sixth generation (6G) technologies and Internet of Things (IoT) are proposed to deploy base stations and IoT devices densely and achieve ultra-high data rate, leading to scarcity of spectrum resource [1]. The symbiotic radio network (SRN) consists of primary communication and backscatter communication, and the symbiotic relationship between them is leveraged as a promising solution for spectrum-efficient IoT communication [2]. In the SRN, primary users (PUs) are authorized to access the licensed spectrum for primary communication, and share the spectrum with backscatter devices (BDs), i.e., IoT devices, for backscatter communication [3].

There are two typical symbiotic radio (SR) setups, i.e., commensal SR (CSR) setup [3]–[7], and parasitic SR (PSR) setup [8]–[10]. In the CSR setup, the symbol rate of backscatter communication is much smaller than that of primary communication [3], [4]. The primary symbol can be viewed as through a slowly varying channel that incorporates BD-related channels. The primary communication may benefit from backscatter communication by treating IoT signals as additional multipath components [6], [7]. In the CSR setup, Jia *et al.* [3] investigated a SR-assisted mobile edge computing network for high-speed railway IoT services, and Wang *et al.* [4] minimized the transmission power subject to the cellular communication outage probability constraints and sum IoT rate constraints. In the SRN with hybrid active-passive communication, Xu *et al.* [5] investigated the weighted sum rate maximization problem and energy efficiency maximization problem. Long *et al.* [6] derived the achievable rates for the primary communication and backscatter communication, and formulated two transmit beamforming optimization problems. Liu *et al.* [7] proposed a paradigm of integrated sensing and communication for the battery-free IoT system, where the meta-material sensors provide additional multipath gain to assist the communication performance. In the PSR setup, Xu *et al.* [8] maximized the system throughput in the SRN, and utilized Bernstein-type inequality to transform the outage rate constraints into deterministic forms. Zhuang *et al.* [9] investigated the hybrid active-passive communication with multi-secondary transmitters, and formulated a throughput maximization problem. In the PSR setup, the symbol rate of backscatter communication is the same or comparable to that of the primary communication [10]. The receiver first decodes the primary signal by treating the backscatter signal as interference, and then decodes the backscatter signal after subtracting the primary signal from the received signal [10], [11]. Thus, the CSR setup outperforms the PSR setup in terms

This work was supported in part by the National Natural Science Foundation of China under Grant 62372413 and Grant 62372412; in part by Zhejiang Provincial Natural Science Foundation of China under Grant No. LZ26F010008; in part by the Fundamental Research Funds for the Provincial Universities of Zhejiang under Grant RF-B2024002; in part by JSPS KAKENHI Grant Numbers JP25K15087; in part by the Project of Cyber Security Establishment with Inter-University Cooperation. *(Corresponding author: Xiaoying Liu.)*

K. Zheng, Z. Li, and X. Liu are with the School of Computer Science and Technology, Zhejiang University of Technology, Hangzhou 310023, China. E-mail: {kechenzheng, 211123120025, xiaoyingliu}@zjut.edu.cn.

J. Liu is with the Center for Strategic Cyber Resilience Research and Development, National Institute of Informatics, Tokyo 101-8430, Japan. E-mail: jliu@nii.ac.jp.

T. Taleb is with the Faculty of Electrical Engineering and Information Technology, Ruhr University Bochum, Bochum 44801, Germany. E-mail: tarik.taleb@rub.de.

N. Shiratori is with the Research and Development Initiative, Chuo University, Tokyo 112-8551, Japan. E-mail: norio.shiratori.e8@tohoku.ac.jp.

of primary communication, while the PSR setup outperforms the CSR setup in terms of backscatter communication [12].

As a promising technique for realizing 6G technologies and IoT network, the cell-free network (CFN) aims to address the challenge of high data rate demands. The CFN eliminates the concept of cell boundaries, and enables access points (APs) to cooperatively serve users, thereby enhancing spatial diversity and improving communication rate [13]. In CFN, APs are randomly distributed in a given area, are connected to a central processing unit (CPU) through fronthaul links, and employ beamforming to configure the transmit power weights of antennas for improving communication rate [14]. Gopal *et al.* [15] proposed three vector quantization approaches for AP placement in CFN to maximize the sum rate of APs. For fairness considerations, Jadidi *et al.* [16] investigated the max-min throughput problem in CFN. Hu *et al.* [17] investigated the CFN with a stacked intelligent metasurface, and maximized the sum rate of users by optimizing beamforming and power allocation.

To address the challenges of high data rate demands and spectrum scarcity in 6G technologies and IoT network, it is a great potential to integrate CFN into SRN, i.e., cell-free SRN (CF-SRN), which leverages macro-diversity to alleviate the double-fading effect, thereby enhancing the symbiotic relationship between the primary communication and backscatter communication. The CF-SRN has been studied in terms of single-BD scenario [18]–[20] and mulit-BD scenario [21], [22]. Dai *et al.* [18] explored the rate regions of primary communication and backscatter communication in the CF-SRN with one BD and PSR setup, and maximized the ergodic rate of backscatter communication. Li *et al.* [19] studied the CF-SRN with one BD and CSR setup, and analyzed the spectrum efficiency under two combining schemes. Lyu *et al.* [20] investigated the CF-SRN with a simultaneously transmitting and reflecting reconfigurable intelligent surface (STAR-RIS), and maximized the system energy efficiency by jointly optimizing the active beamforming of APs and reflection beamforming of the STAR-RIS. Works [18]–[20] studied the CF-SRN with one BD where the double-fading effect degrades the backscatter link, while works [21] and [22] improved the passive communication rate of the CF-SRN with multi-BD. In [21], Dai *et al.* studied the CF-SRN with multi-reconfigurable intelligent surface and CSR setup, and formulated a passive communication rate maximization problem. Li *et al.* [22] proposed the CF-SRN with multi-user, multi-BD and CSR setup, and investigated the viability of employing rate splitting multiple access to alleviate interference among users.

Existing works [3]–[5], [7]–[9], [18]–[22] focus on the SRN with single CSR or PSR setup, while the potential benefits of integrating the advantage of CSR setup in terms of primary communication and that of PSR setup in terms of backscatter communication could be explored. In addition, with respect to the hybrid CSR-active communication (AC) in [5] and the hybrid PSR-AC in [9], we are motivated to investigate the potential of the hybrid CSR-PSR setup and AC. Therefore we investigate the CF-SRN with hybrid CSR-PSR setup and AC that balances the tradeoff between primary communication and backscatter communication from the perspective of time. In the CF-SRN, we design a time slot structure that includes the channel estimation (CE) phase, CSR phase, PSR phase, and AC phase. The BDs split the energy of primary radio frequency (RF) signals to perform backscatter communication and energy harvesting (EH) during the CSR phase and PSR phase, and consume the harvested energy to perform AC during the AC phase. Adjusting the backscatter coefficients of BDs balances the tradeoff between backscatter communication and EH, while optimizing the beamforming of APs balances the tradeoff between primary communication and backscatter communication from the perspective of power. The main contributions are summarized as follows.

- We propose a novel hybrid CSR-PSR setup for the CF-SRN, where BDs are equipped with multi-antenna and AC capability. We adopt a two-stage CE method to obtain the estimated channels and CE errors. We formulate the sum backscatter throughput maximization problem by optimizing the time allocation vector, beamforming vectors of the APs and BDs, and reflection coefficients of the BDs, subject to the minimum sum primary throughput constraint. The formulated problem with coupled high-dimensional variables is non-convex.
- To solve it, we first use Jensen's inequality to transform the formulated problem that includes expectations over random CE errors into a deterministic form, and then propose a block coordinate descent (BCD)-based semi-definite relaxation (SDR) and successive convex approximation (SCA) algorithm, i.e., BSS algorithm. To be specific, we propose the BCD method that decomposes the formulated problem into time allocation optimization (TAO) subproblem, beamforming optimization (BO) subproblem, and reflection coefficient optimization (RCO) subproblem. We adopt the linear programming (LP) method to obtain the optimal solution of TAO subproblem, utilize the SDR method to equivalently transform BO subproblem and RCO subproblem into non-convex SDR problems, and utilize the SCA method to address the non-convexity resulted from fractional structures.
- Simulation results validate the superiority of the proposed BSS algorithm and hybrid CSR-PSR setup. Simulation results show that, sum backscatter throughput in the hybrid CSR-PSR setup is larger than that in the CSR setup, and sum primary throughput in the hybrid CSR-PSR setup is larger than that in the PSR setup.

The rest of this paper is organized as follows. In Section II, we introduce the system model. In Section III, we formulate and analyze the sum backscatter throughput maximization problem. In Section IV, we propose the BSS algorithm to solve the formulated problem. In Section V, we present simulation results and discussions. Section VI concludes this paper.

The major notations in this paper are listed as follows: lowercase letters, such as a, represent scalars, boldface lowercase letters, such as $\mathbf{a}$, represent vectors, and boldface uppercase letters, such as $\mathbf{A}$, represent matrices. For scalar a, $|a|$ represents the absolute value of a. For vector $\mathbf{a}$, $\mathbf{a}^{\mathrm{T}}$ represents the transpose of $\mathbf{a}$, $\mathbf{a}^{\mathrm{H}}$ represents the conjugate transpose of $\mathbf{a}$, and $\|\mathbf{a}\|$ represents the Frobenius norm of $\mathbf{a}$. For matrix

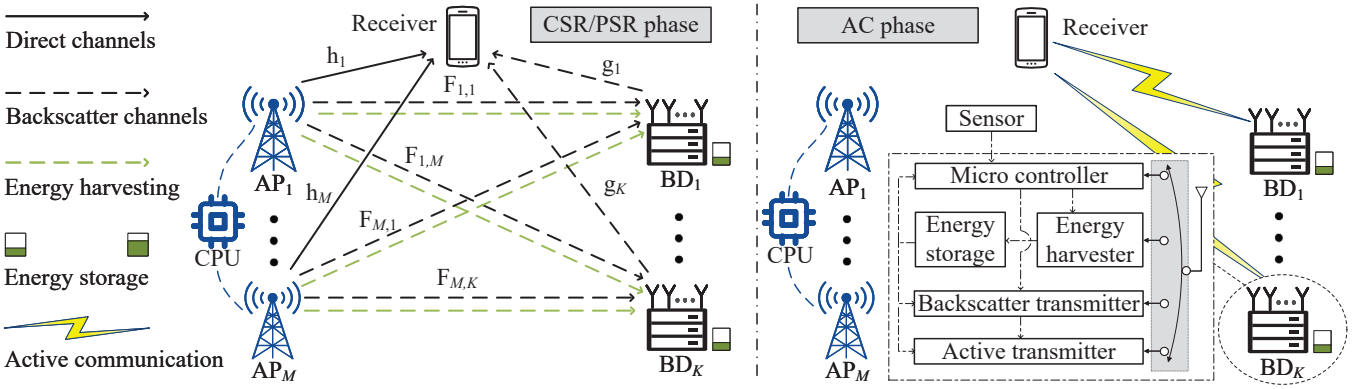

Fig. 1. System model of the CF-SRN.

TABLE I
LIST OF PARAMETERS (PARA.)

Para.	Definition
M	Number of APs
K	Number of BDs
Q	Number of antennas at each AP
L	Number of antennas at each BD
c_k	Backscatter symbol of BD_k during CSR phase
$c_k(n)$	n-th backscatter symbol of BD_k during PSR phase
$\mathbf{h}_m$	Direct link MISO channels from AP_m to the receiver
$\hat{\mathbf{h}}_m$	Estimation of $\mathbf{h}_m$
$\tilde{\mathbf{h}}_m$	Estimation error of $\mathbf{h}_m$
$\mathbf{F}_{m,k}$	Forward-link MIMO channels from AP_m to BD_k
$\mathbf{g}_k$	Backward-link MISO channels from BD_k to the receiver
$\mathbf{v}_{m,k}$	Cascaded channels from AP_m via BD_k to the receiver
$\hat{\mathbf{v}}_{m,k}$	Estimation of $\mathbf{v}_{m,k}$
$\tilde{\mathbf{v}}_{m,k}$	Estimation error of $\mathbf{v}_{m,k}$
$\mathbf{w}_m^C$	Transmit beamforming vector of AP_m during CSR phase
$\mathbf{w}_m^P$	Transmit beamforming vector of AP_m during PSR phase
$\mathbf{w}_k^A$	Transmit beamforming vector of BD_k during AC phase
P_m	Maximum transmit power of AP_m
E_k^{total}	Total harvested energy of BD_k
R^C	Throughput of primary transmission during CSR phase
$R_{b,k}^C$	Throughput of BD_k during CSR phase
R^P	Throughput of primary transmission during PSR phase
$R_{b,k}^P$	Throughput of BD_k during PSR phase
α_k	Reflection coefficient of BD_k

$\mathbf{A}$, $\text{Tr}(\mathbf{A})$ represents the trace of $\mathbf{A}$, $\text{Rank}(\mathbf{A})$ represents the rank of $\mathbf{A}$, $\mathbf{A}^{\text{T}}$ represents the transpose of $\mathbf{A}$, and $\mathbf{A}^{\text{H}}$ represents the conjugate transpose of $\mathbf{A}$. $\text{Diag}(\mathbf{A})$ represents a diagonal matrix where the diagonal elements correspond exactly to the main diagonal elements of $\mathbf{A}$. $\mathbf{A} \succeq 0$ represents that $\mathbf{A}$ is a positive semi-definite matrix. $\mathbf{I}_N$ denotes the $N \times N$ identity matrix. $\mathbb{C}^{x \times y}$ denotes the space of $x \times y$ complex-valued matrices. $\mathbb{E}_X[\cdot]$ denotes the expectation with respect to X. $\mathcal{CN}(\mu, \sigma^2)$ represents the circularly symmetric complex Gaussian (CSCG) distribution with mean μ and variance σ^2. For readability, we summarize the key parameters in Table I.

II. System Model

We introduce the system model from four aspects: network model, time slot structure, CE, and communication model.

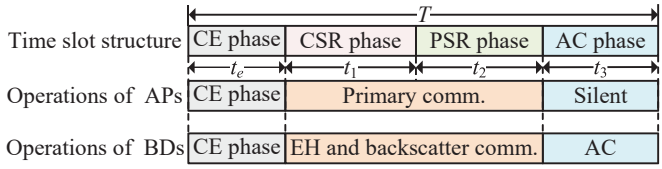

Fig. 2. Time slot structure.

A. Network Model

As shown in Fig. 1, we study a CF-SRN that consists of the CFN and IoT network, and includes M APs denoted by set $\mathcal{M} = \{1, \ldots, M\}$, K BDs denoted by set $\mathcal{K} = \{1, \ldots, K\}$, and one single-antenna receiver. Each AP is equipped with Q antennas, and is connected to the CPU. Each BD is equipped with L antennas, and is connected to a sensor that collects environmental data. Similar to [23] and [5], we consider that each BD contains an energy harvester, an energy storage, a backscatter transmitter, an active transmitter, and a micro-controller. The energy harvester harvests the energy of the ambient RF signals and stores it in the energy storage. The backscatter transmitter performs signal modulation to transmit backscatter signals by adjusting the impedance. The active transmitter transmits the RF signals by consuming the harvested energy, and the micro-controller schedules the operation. Each BD can simultaneously perform EH and backscatter communication by splitting the energy of RF signals. The CF-SRN is suitable for IoT applications such as healthcare IoT [24] and smart home scenario.

As shown in Fig. 1, the APs transmit primary RF signals to the receiver through the direct-link channels and the cascaded backscatter-link channels from the APs via BDs to the receiver. The cascaded backscatter-link channels consist of the forward-link channels from the APs to the BDs and the backward-link channels from the BDs to the receiver. Let $\mathbf{h}_m \in \mathbb{C}^{Q \times 1}$ represent the direct-link multiple-input single-output (MISO) channels from AP_m to the receiver, $\mathbf{F}_{m,k} \in \mathbb{C}^{L \times Q}$ represent the forward-link multiple-input multiple-output channels from AP_m to BD_k, and $\mathbf{g}_k \in \mathbb{C}^{L \times 1}$ represent the backward-link MISO channels from BD_k to the receiver. The cascaded backscatter-link channels from AP_m via BD_k to the receiver,

denoted by $\mathbf{v}_{m,k} \in \mathbb{C}^{Q\times 1}$, are given by

$$\mathbf{v}_{m,k} = \mathbf{F}_{m,k}^{\mathrm{H}} \mathbf{g}_k. \tag{1}$$

We formulate the channel gain in the CF-SRN by both large-scale channel gain and small-scale channel gain. The large-scale channel gain of $\mathbf{h}_m$ is modeled as $\varepsilon_m = \beta d_{m,r}^{-\gamma}$, where β denotes the reference channel coefficient, $d_{m,r}$ denotes the distance between AP$_m$ and the receiver, and γ denotes the path loss exponent. The large-scale channel gain of $\mathbf{F}_{m,k}$ is modeled as $\nu_{m,k} = \beta d_{m,k}^{-\gamma}$, and that of $\mathbf{g}_k$ is modeled as $\epsilon_k = \beta d_{k,r}^{-\gamma}$, where $d_{m,k}$ denotes the distance between AP$_m$ and BD$_k$, and $d_{k,r}$ denotes the distance between BD$_k$ and the receiver. The small-scale fading coefficients follow the independent and identically distributed (i.i.d.) CSCG distribution with mean 0 and variance 1, and we have $\mathbf{h}_m \sim \mathcal{CN}(0, \mathbf{Q}_m)$, $\mathbf{g}_k \sim \mathcal{CN}(0, \mathbf{U}_k)$, and $\mathbf{v}_{m,k} \sim \mathcal{CN}(0, \mathbf{Q}_{m,k})$, where $\mathbf{Q}_m = \varepsilon_m \mathbf{I}_Q$, $\mathbf{U}_k = \epsilon_k \mathbf{I}_L$, and $\mathbf{Q}_{m,k} = L\nu_{m,k}\epsilon_k \mathbf{I}_Q$ are covariance matrices of $\mathbf{h}_m$, $\mathbf{g}_k$, and $\mathbf{v}_{m,k}$, respectively.

B. Time Slot Model

As shown in Fig. 2, we consider a time slot structure for the CF-SRN, where each time slot with equal duration T is divided into four phases: the CE phase with duration t_e, the CSR phase with duration t_1, the PSR phase with duration t_2, and the AC phase with duration t_3. The duration of the CE phase is sufficiently short to be negligible, and we will discuss the process of CE in Section II-C. The duration of the CSR phase, that of the PSR phase, and that of the AC phase satisfy

$$t_1 + t_2 + t_3 < T. \tag{2}$$

During the CSR phase and PSR phase, the APs perform primary communication by collaboratively transmitting primary RF signals to the receiver through the direct-link channels and cascaded backscatter-link channels, and the BDs backscatter the RF signals from the APs to the receiver while simultaneously performing EH. During the AC phase, when the required throughput of the APs is satisfied, the APs remain silent. The micro-controller of the BD switches the circuit to the active transmitter, and the BDs perform AC by consuming the harvested energy to transmit the environmental IoT data to the receiver. It is noted that, the BDs considered in this paper require the capability of adjusting the RF switching frequency at runtime [25] and supporting AC [5], which inevitably increases hardware complexity.

During the CSR phase, we consider the CSR setup [6] as

$$T_b = NT_p, \tag{3}$$

where N represents the integer spreading factor that satisfies $N \gg 1$, T_b represents the symbol period of backscatter communication, and T_p represents that of primary communication. c_k represents the backscatter symbol transmitted by BD$_k$ to the receiver through the backward-link channels, and is modulated by using phase-shift keying (PSK) modulation with mean 0 and variance 1. For $n = 1, \ldots, N$, let $s(n)$ be the n-th primary symbol during one backscatter symbol period, and $s(n) \sim \mathcal{CN}(0, 1)$ holds. According to (3), the symbol period of c_k is longer than that of $s(n)$. According to [26], when BDs adopt PSK modulation during the CSR phase, backscatter communication may not enhance the primary communication. To be specific, if the phase of the BD's reflection coefficient is not set appropriately, backscatter communication can even be detrimental to the primary throughput. Due to the superposition channels of APs and BDs, it is challenging to optimize the phases of the BDs' reflection coefficients. In the future work, we would like to study the impact of the constraint that the primary throughput with the assistance of backscatter communication is larger than that of the standalone primary communication on the throughput performance.

In primary communication, $s(n)$ is transmitted from the APs to the receiver through direct-link channels and cascaded backscatter-link channels. During the CSR phase, the received signal at the receiver, denoted by $y^C(n)$, is

$$y^C(n) = \sum_{m=1}^{M} \mathbf{h}_m^{\mathrm{H}} \mathbf{w}_m^C s(n) + \sum_{m=1}^{M}\sum_{k=1}^{K} \sqrt{\alpha_k} c_k \mathbf{v}_{m,k}^{\mathrm{H}} \mathbf{w}_m^C s(n) + z(n), \tag{4}$$

where $\mathbf{w}_m^C \in \mathbb{C}^{Q\times 1}$ denotes the beamforming vector of AP$_m$, and α_k denotes the reflection coefficient of BD$_k$. On the right hand side of the equality in (4), the first term represents the accumulated direct-link signals from the APs, the second term represents the accumulated backscatter-link signals from the APs via BDs, and $z(n)$ represents the additive white Gaussian noise (AWGN) with mean 0 and variance σ^2. As the gains of the cascaded backscatter-link channels are generally smaller than those of the direct-link channels due to the double-path fading, the receiver applies the successive interference cancellation (SIC) technique to decode $s(n)$. In practical scenarios, decoding c_k at the receiver by using SIC results in residual interferences due to imperfect cancellation, i.e., imperfect SIC, which degrades the corresponding signal to interference plus noise ratio (SINR) and sum backscatter throughput. To simplify the analysis, we neglect the residual interference caused by the imperfect SIC. By subtracting the direct-link signals from (4), the receiver obtains intermediate signal, denoted by $y_b^C(n)$, as

$$y_b^C(n) = \sum_{m=1}^{M}\sum_{k=1}^{K} \sqrt{\alpha_k} c_k \mathbf{v}_{m,k}^{\mathrm{H}} \mathbf{w}_m^C s(n) + z(n). \tag{5}$$

$\mathbf{y}_b^C = \left[y_b^C(1), \ldots, y_b^C(N)\right]^{\mathrm{T}}$ represents the vector form of the intermediate signals in one backscatter symbol period as

$$\mathbf{y}_b^C = \sum_{m=1}^{M} \sqrt{\alpha_k} \mathbf{v}_{m,k}^{\mathrm{H}} \mathbf{w}_m^C \mathbf{s} c_k + \sum_{m=1}^{M}\sum_{i\neq k}^{K} \sqrt{\alpha_i} \mathbf{v}_{m,i}^{\mathrm{H}} \mathbf{w}_m^C \mathbf{s} c_i + \mathbf{z}, \tag{6}$$

where $\mathbf{s} = [s(1), \ldots, s(N)]^{\mathrm{T}}$ represents the primary symbol vector, and $\mathbf{z} = [z(1), \ldots, z(N)]^{\mathrm{T}}$ represents the noise vector. On the right hand side of the equality in (6), the first term represents the accumulated backscatter-link signals of BD$_k$, and the second term represents those of the other BDs.

During the CSR phase, we adopt a linear EH model [28], the received power by BD$_k$ from the APs is $P_{b,k}^C = \| \sum_{m=1}^{M} \mathbf{F}_{m,k} \mathbf{w}_m^C \|^2$, and the total amount of the harvested

energy, denoted by E_k^C, is expressed as

$$E_k^C = (1-\alpha_k)\, t_1 \eta P_{b,k}^C, \tag{7}$$

where $\eta \in (0,1)$ denotes the EH efficiency coefficient.

During the PSR phase, we consider the PSR setup, i.e., the symbol period of the n-th primary symbol $s(n)$ is equal to that of $c_k(n)$, $N=1$ holds [6], and the received signal at the receiver is

$$y^P(n) = \sum_{m=1}^{M} \mathbf{h}_m^{\mathrm{H}} \mathbf{w}_m^P s(n) + \sum_{m=1}^{M}\sum_{k=1}^{K} \sqrt{\alpha_k}\mathbf{v}_{m,k}^{\mathrm{H}} \mathbf{w}_m^P s(n) c_k(n) + z(n), \tag{8}$$

where $\mathbf{w}_m^P$ denotes the beamforming vector of AP$_m$ during the PSR phase. On the right hand side of the equality in (8), the first term represents the accumulated direct-link signals, and the second term represents the accumulated backscatter-link signals. By subtracting the accumulated direct-link signals $\sum_{m=1}^{M} \mathbf{h}_m^{\mathrm{H}} \mathbf{w}_m^P s(n)$ from (8) through the SIC technique, the receiver obtains the intermediate signal during the PSR phase, denoted by $y_b^P(n)$, as

$$y_b^P(n) = \sum_{m=1}^{M} \sqrt{\alpha_k}\mathbf{v}_{m,k}^{\mathrm{H}} \mathbf{w}_m^P s(n) c_k(n) + \sum_{m=1}^{M}\sum_{i\neq k}^{K} \sqrt{\alpha_i}\mathbf{v}_{m,i}^{\mathrm{H}} \mathbf{w}_m^P s(n) c_i(n) + z(n). \tag{9}$$

The power of the signals from APs to BD$_k$ during the PSR phase is $P_{b,k}^P = \| \sum_{m=1}^{M} \mathbf{F}_{m,k} \mathbf{w}_m^P \|^2$, and the total amount of the harvested energy, denoted by E_k^P, is expressed as

$$E_k^P = (1-\alpha_k)\, t_2 \eta P_{b,k}^P. \tag{10}$$

Based on (7) and (10), the total amount of the energy harvested by BD$_k$ during the CSR phase and PSR phase is

$$E_k^{\text{total}} = E_k^C + E_k^P. \tag{11}$$

During the AC phase, the BDs transmit the environmental IoT data to the receiver. Due to the advantages of high spectrum efficiency and massive connectivity for IoT networks [29], we adopt the uplink non-orthogonal multiple access (NOMA) scheme for the communication from the BDs to the receiver. In the uplink NOMA scheme, the SIC technique is implemented by the receiver to decode the backward-link signal of the BDs in descending order of channel gains $\mathbf{g}_k$, $k \in \mathcal{K}$. The backward-link signal of the BD with the largest channel gain is decoded at first, and subtracted by the receiver. Without loss of generality, the backward-link channels are numbered in descending order of channel gains as $\|\mathbf{g}_1\|^2 \geq \cdots \geq \|\mathbf{g}_K\|^2$. During the AC phase, the throughput of BD$_k$ to the receiver, denoted by $R_{b,k}^A$, is expressed as

$$R_{b,k}^A = B t_3 \log_2\left(1 + \frac{\left|\mathbf{g}_k^{\mathrm{H}} \mathbf{w}_k^A\right|^2}{\sum_{i>k}^{K} \left|\mathbf{g}_i^{\mathrm{H}} \mathbf{w}_i^A\right| + \sigma^2}\right), \tag{12}$$

where B denotes the bandwidth, $\mathbf{w}_k^A$ denotes the beamforming vector of BD$_k$ during the AC phase. The sum throughput of BDs during the AC phase, denoted by R_{sum}^A, is expressed as

$$R_{\text{sum}}^A = B t_3 \log_2\left(1 + \frac{\sum_{k=1}^{K} \left|\mathbf{g}_k^{\mathrm{H}} \mathbf{w}_k^A\right|^2}{\sigma^2}\right). \tag{13}$$

C. The Process of CE

As the channel state information (CSI) has an important impact on the network performance, we estimate direct-link channels and cascaded backscatter-link channels. Due to the advantage of avoiding mutual interference between the direct-link channels and cascaded backscatter-link channels [19], we adopt the two-stage CE method. During the first stage of CE, the BDs remain silent, while the APs receive the training pilot sequence from the receiver, and transmit the training pilot sequence to the CPU through fronthaul links. Let $\boldsymbol{\varphi}_1 \in \mathbb{C}^{\tau_1 \times 1}$ denote the training pilot sequence during the first stage of CE, where $\boldsymbol{\varphi}_1^{\mathrm{H}} \boldsymbol{\varphi}_1 = \tau_1$ holds. The received signal at AP$_m$ that corresponds to $\boldsymbol{\varphi}_1$, denoted by $\mathbf{Y}_m$, is

$$\mathbf{Y}_m = \sqrt{P_t}\mathbf{h}_m \boldsymbol{\varphi}_1^{\mathrm{H}} + \mathbf{Z}_m, \tag{14}$$

where P_t denotes the training power, and $\mathbf{Z}_m \in \mathbb{C}^{Q \times \tau_1}$ denotes the i.i.d. CSCG noise with mean 0 and variance σ^2.

As the APs have knowledge of the training pilot sequence $\boldsymbol{\varphi}_1$ and training power P_t, they simplify $\mathbf{Y}_m$ in (14) by right-multiplying both sides of (14) by $\frac{\boldsymbol{\varphi}_1}{\sqrt{P_t}}$ as

$$\check{\mathbf{y}}_m = \tau_1 \mathbf{h}_m + \frac{\check{\mathbf{z}}_m}{\sqrt{P_t}}, \tag{15}$$

where $\check{\mathbf{y}}_m = \mathbf{Y}_m \frac{\boldsymbol{\varphi}_1}{\sqrt{P_t}}$ and $\check{\mathbf{z}}_m = \mathbf{Z}_m \boldsymbol{\varphi}_1$ hold, and $\check{\mathbf{z}}_m \sim \mathcal{CN}(0, \tau_1 \sigma^2 \mathbf{I}_Q)$ denotes the CSCG noise with mean 0 and variance $\tau_1\sigma^2$. Under the imperfect CSI estimation, we use the linear minimum mean square error (LMMSE) CE [30] to express $\mathbf{h}_m$ as

$$\mathbf{h}_m = \hat{\mathbf{h}}_m + \tilde{\mathbf{h}}_m, \tag{16}$$

where $\hat{\mathbf{h}}_m$ denotes the estimation of $\mathbf{h}_m$, and $\tilde{\mathbf{h}}_m$ denotes the estimation error of $\mathbf{h}_m$. We have $\hat{\mathbf{h}}_m$ as

$$\hat{\mathbf{h}}_m = \mathbb{E}\left[\mathbf{h}_m \check{\mathbf{y}}_m^{\mathrm{H}}\right] \mathbb{E}\left[\check{\mathbf{y}}_m \check{\mathbf{y}}_m^{\mathrm{H}}\right]^{-1} \check{\mathbf{y}}_m = \frac{P_t \mathbf{Q}_m}{\tau_1 P_t \mathbf{Q}_m + \sigma^2 \mathbf{I}_Q} \check{\mathbf{y}}_m. \tag{17}$$

For ease of notation, we let $\frac{P_t \mathbf{Q}_m}{\tau_1 P_t \mathbf{Q}_m + \sigma^2 \mathbf{I}_Q} = \boldsymbol{\Upsilon}_m$. According to (16) and (17), we obtain $\hat{\mathbf{h}}_m \sim \mathcal{CN}(0, \boldsymbol{\Gamma}_m)$ and $\tilde{\mathbf{h}}_m \sim \mathcal{CN}(0, \mathbf{C}_m)$, where $\boldsymbol{\Gamma}_m = \tau_1 \mathbf{Q}_m \boldsymbol{\Upsilon}_m$, and $\mathbf{C}_m = \mathbf{Q}_m - \boldsymbol{\Gamma}_m$.

During the second stage of CE, the APs receive the uplink training pilot sequence backscattered by BD$_k$ from the receiver, while the other BDs remain silent, and then transmit it to the CPU via fronthaul links. Similar to the first stage of CE, we use the LMMSE CE model to express $\mathbf{v}_{m,k}$ as

$$\mathbf{v}_{m,k} = \hat{\mathbf{v}}_{m,k} + \tilde{\mathbf{v}}_{m,k}, \tag{18}$$

where $\hat{\mathbf{v}}_{m,k}$ denotes the estimation of $\mathbf{v}_{m,k}$, and $\tilde{\mathbf{v}}_{m,k}$ denotes the estimation error of $\mathbf{v}_{m,k}$.

Let $\boldsymbol{\varphi}_2 \in \mathbb{C}^{\tau_2 \times 1}$ denote the training pilot sequence during the second stage of CE, where $\boldsymbol{\varphi}_2^{\mathrm{H}} \boldsymbol{\varphi}_2 = \tau_2$ and $\frac{P_t \alpha_k \mathbf{Q}_{m,k}}{\tau_2 P_t \alpha_k \mathbf{Q}_{m,k} + P_t \tau_2 \mathbf{C}_m + \sigma^2 \mathbf{I}_Q} = \boldsymbol{\Psi}_{m,k}$ hold. Then we have $\hat{\mathbf{v}}_{m,k} \sim \mathcal{CN}(0, \boldsymbol{\xi}_{m,k})$ and $\tilde{\mathbf{v}}_{m,k} \sim \mathcal{CN}(0, \mathbf{C}_{m,k})$, where $\boldsymbol{\xi}_{m,k} = \tau_2 \mathbf{Q}_{m,k} \boldsymbol{\Psi}_{m,k}$ and $\mathbf{C}_{m,k} = \mathbf{Q}_{m,k} - \boldsymbol{\xi}_{m,k}$ hold.

D. Communication Model

Considering the estimated channels $\hat{\mathbf{h}}_m$, $\hat{\mathbf{v}}_{m,k}$, and CE errors $\tilde{\mathbf{h}}_m$, $\tilde{\mathbf{v}}_{m,k}$, we formulate the throughput of APs and that of BDs during the CSR phase and PSR phase, respectively. According to (16) and (18), the received signal at the receiver during the CSR phase in (4) is rewritten as

$$y^C(n) = \sum_{m=1}^{M} \left(\hat{\mathbf{h}}_m + \sum_{k=1}^{K} \sqrt{\alpha_k} c_k \hat{\mathbf{v}}_{m,k}\right)^{\mathrm{H}} \mathbf{w}_m^C s(n) + \sum_{m=1}^{M} \left(\tilde{\mathbf{h}}_m + \sum_{k=1}^{K} \sqrt{\alpha_k} c_k \tilde{\mathbf{v}}_{m,k}\right)^{\mathrm{H}} \mathbf{w}_m^C s(n) + z(n). \quad (19)$$

The receiver decodes the primary and backscatter symbols according to $y^C(n)$ in (19). For the receiver, the first term on the right hand side of the equality in (19) is the desired signal, and the second term is viewed as the interference. During the duration of N primary symbol periods in the CSR setup, c_k remains constant. According to (3) and (19), $s(n)$ can be viewed to go through a slowly varying channel $\sum_{k=1}^{K} \sqrt{\alpha_k} c_k \hat{\mathbf{v}}_{m,k}$, and the equivalent channel for decoding $s(n)$ is denoted by $\hat{\mathbf{h}}_m + \sum_{k=1}^{K} \sqrt{\alpha_k} c_k \hat{\mathbf{v}}_{m,k}$, which includes the direct-link channels and the cascaded backscatter-link channels. The ergodic capacity of this channel can be characterized by averaging over all possible channel states [31]. As the CE errors $\tilde{\mathbf{h}}_m$ and $\tilde{\mathbf{v}}_{m,k}$ are random parameters [18], we obtain throughput of APs during the CSR phase by taking the expectations of c_k, $\tilde{\mathbf{h}}_m$, and $\tilde{\mathbf{v}}_{m,k}$, denoted by R^C, as

$$R^C = t_1 B \mathbb{E}_{c_k, \tilde{\mathbf{h}}_m, \tilde{\mathbf{v}}_{m,k}} \left[\log_2(1+\gamma^C)\right], \quad (20)$$

where

$$\gamma^C = \frac{\left| \sum_{m=1}^{M} \left(\hat{\mathbf{h}}_m + \sum_{k=1}^{K} \sqrt{\alpha_k} c_k \hat{\mathbf{v}}_{m,k}\right)^{\mathrm{H}} \mathbf{w}_m^C \right|^2}{\left| \sum_{m=1}^{M} \left(\tilde{\mathbf{h}}_m + \sum_{k=1}^{K} \sqrt{\alpha_k} c_k \tilde{\mathbf{v}}_{m,k}\right)^{\mathrm{H}} \mathbf{w}_m^C \right|^2 + \sigma^2} \quad (21)$$

represents the SINR of the receiver decoding $s(n)$. Let $\mathcal{C}$ denote the set of random backscatter symbols, and $\mathbf{c} = [c_1, \ldots, c_K]$ represent the backscatter symbol vector of the BDs during the CSR phase. By taking the expectation of c_k in (20), we formulate the throughput of APs with expectations of $\tilde{\mathbf{h}}_{\mathbf{m}}$ and $\tilde{\mathbf{v}}_{m,k}$ during the CSR phase as [27]

$$R^C = \frac{t_1 B}{p^K} \sum_{\mathbf{c} \in \mathcal{C}} \mathbb{E}_{\tilde{\mathbf{h}}_m, \tilde{\mathbf{v}}_{m,k}} \left[\log_2\left(1+\gamma^C(\mathbf{c})\right)\right], \quad (22)$$

where p denotes the number of signal states of the BDs that adopt PSK modulation, e.g., when $p = 2$, the BDs adopt binary PSK modulation.

Then we formulate the throughput of BDs during the CSR phase. After decoding $s(n)$, the receiver subtracts the accumulated direct-link signals $\sum_{m=1}^{M} \hat{\mathbf{h}}_m^{\mathrm{H}} \mathbf{w}_m^C s(n)$ from (19), and then the intermediate signal in (6), can be rewritten as

$$\mathbf{y}_b^C = \sum_{m=1}^{M} \sqrt{\alpha_k} \hat{\mathbf{v}}_{m,k}^{\mathrm{H}} \mathbf{w}_m^C \mathbf{s} c_k + \sum_{m=1}^{M} \sum_{i \neq k}^{K} \sqrt{\alpha_i} \hat{\mathbf{v}}_{m,i}^{\mathrm{H}} \mathbf{w}_m^C \mathbf{s} c_i + \sum_{m=1}^{M} \left(\tilde{\mathbf{h}}_m + \sum_{k=1}^{K} \sqrt{\alpha_k} c_k \tilde{\mathbf{v}}_{m,k}\right)^{\mathrm{H}} \mathbf{w}_m^C \mathbf{s} + \mathbf{z}. \quad (23)$$

For the receiver decoding the backscatter symbols, the first term on the right hand side of the equality in (23) is the desired signal, the second and third terms are viewed as the interference. In the CSR setup, according to (3), the primary symbol $s(n)$ is viewed as a spread-spectrum code with length N for the backscatter symbol. Then the receiver leverages the maximal ratio combining (MRC) to enhance the SINR when decoding the backscatter symbols. Similar to [22] and [32], we use the Shannon capacity to formulate the throughput of BD_k with PSK modulation. The SIC technique is implemented by the receiver to decode the backscatter symbols in descending order of the channel gains $\sum_{m=1}^{M} \hat{\mathbf{v}}_{m,k}$, $k \in \mathcal{K}$. The throughput of BD_k during the CSR phase, denoted by $R_{b,k}^C$, is expressed as

$$R_{b,k}^C = \frac{t_1 B}{N} \mathbb{E}_{\tilde{\mathbf{h}}_m, \tilde{\mathbf{v}}_{m,k}} \left[\log_2(1+\gamma_{b,k}^C)\right], \quad (24)$$

where $\frac{1}{N}$ is due to (3), $\gamma_{b,k}^C$ denotes the SINR of the receiver decoding the backscatter symbols of BD_k in (25), and ϑ denotes the performance gap between the Shannon capacity and the PSK modulation with $0 < \vartheta < 1$ [33]. The sum throughput of BDs during the CSR phase, denoted by R_{sum}^C, is accordingly given by (26).

During the PSR phase, similar to (19), the received signal at the receiver in (8), i.e., $y^P(n)$, is expressed as

$$y^P(n) = \sum_{m=1}^{M} \hat{\mathbf{h}}_m^{\mathrm{H}} \mathbf{w}_m^P s(n) + \sum_{k=1}^{K} \sum_{m=1}^{M} \sqrt{\alpha_k} \hat{\mathbf{v}}_{m,k}^{\mathrm{H}} \mathbf{w}_m^P s(n) c_k(n) + \sum_{m=1}^{M} \left(\tilde{\mathbf{h}}_m + \sum_{k=1}^{K} \sqrt{\alpha_k} c_k(n) \tilde{\mathbf{v}}_{m,k}\right)^{\mathrm{H}} \mathbf{w}_m^P s(n) + z(n). \quad (27)$$

For the receiver decoding the primary symbols, the first term on the right hand side of the equality in (27) is the desired signal. In the PSR setup, the throughput of APs during the PSR phase, denoted by R^P, is expressed as

$$R^P = t_2 B \mathbb{E}_{\tilde{\mathbf{h}}_m, \tilde{\mathbf{v}}_{m,k}} \left[\log_2(1+\gamma^P)\right], \quad (28)$$

where γ^P denotes the SINR of the receiver decoding the primary symbol in (29).

Then we formulate the throughput of BDs during the PSR phase. Similar to the decoding process during the CSR phase, the intermediate signal in (9) is

$$y_b^P(n) = \sum_{m=1}^{M} \sqrt{\alpha_k} \hat{\mathbf{v}}_{m,k}^{\mathrm{H}} \mathbf{w}_m^P s(n) c_k(n) + \sum_{i \neq k}^{K} \sum_{m=1}^{M} \sqrt{\alpha_i} \hat{\mathbf{v}}_{m,i}^{\mathrm{H}} \mathbf{w}_m^P s(n) c_i(n) + z(n) + \sum_{m=1}^{M} \left(\tilde{\mathbf{h}}_m + \sum_{k=1}^{K} \sqrt{\alpha_k} c_k(n) \tilde{\mathbf{v}}_{m,k}\right)^{\mathrm{H}} \mathbf{w}_m^P s(n). \quad (30)$$

For the receiver decoding the backscatter symbols, the first term on the right hand side of the equality in (30) is the desired signal, the other terms are viewed as the interference. The SIC technique is implemented by the receiver to decode the backscatter symbols in descending order of the channel gains $\sum_{m=1}^{M} \hat{\mathbf{v}}_{m,k}$, $k \in \mathcal{K}$, and the throughput of BD_k during the PSR phase, denoted by $R_{b,k}^P$, is expressed as

$$R_{b,k}^P = t_2 B \mathbb{E}_{\tilde{\mathbf{h}}_m, \tilde{\mathbf{v}}_{m,k}} \left[\log_2(1+\gamma_{b,k}^P)\right], \quad (31)$$

where $\gamma_{b,k}^P$ denotes the SINR of the receiver decoding the

$$\gamma_{b,k}^{C}=\frac{\vartheta N\left|\sum_{m=1}^{M}\sqrt{\alpha_k}\hat{\mathbf{v}}_{m,k}^{\mathrm{H}}\mathbf{w}_m^{C}\right|^2}{N\left|\sum_{m=1}^{M}\left(\tilde{\mathbf{h}}_m+\sum_{k=1}^{K}\sqrt{\alpha_k}\tilde{\mathbf{v}}_{m,k}\right)^{\mathrm{H}}\mathbf{w}_m^{C}\right|^2+N\sum_{i>k}^{K}\left|\sum_{m=1}^{M}\sqrt{\alpha_i}\hat{\mathbf{v}}_{m,i}^{\mathrm{H}}\mathbf{w}_m^{C}\right|^2+\sigma^2}. \tag{25}$$

$$R_{\text{sum}}^{C}=\frac{t_1 B}{N}\mathbb{E}_{\tilde{\mathbf{h}}_m,\tilde{\mathbf{v}}_{m,k}}\left[\log_2\left(1+\frac{\vartheta N\sum_{k=1}^{K}\left|\sum_{m=1}^{M}\sqrt{\alpha_k}\hat{\mathbf{v}}_{m,k}^{\mathrm{H}}\mathbf{w}_m^{C}\right|^2}{N\left|\sum_{m=1}^{M}\left(\tilde{\mathbf{h}}_m+\sum_{k=1}^{K}\sqrt{\alpha_k}\tilde{\mathbf{v}}_{m,k}\right)^{\mathrm{H}}\mathbf{w}_m^{C}\right|^2+\sigma^2}\right)\right]. \tag{26}$$

$$\gamma^{P}=\frac{\left|\sum_{m=1}^{M}\hat{\mathbf{h}}_m^{\mathrm{H}}\mathbf{w}_m^{P}\right|^2}{\left|\sum_{m=1}^{M}\left(\tilde{\mathbf{h}}_m+\sum_{k=1}^{K}\sqrt{\alpha_k}\tilde{\mathbf{v}}_{m,k}\right)^{\mathrm{H}}\mathbf{w}_m^{P}\right|^2+\sum_{k=1}^{K}\left|\sum_{m=1}^{M}\sqrt{\alpha_k}\hat{\mathbf{v}}_{m,k}^{\mathrm{H}}\mathbf{w}_m^{P}\right|^2+\sigma^2}. \tag{29}$$

$$\gamma_{b,k}^{P}=\frac{\vartheta\left|\sum_{m=1}^{M}\sqrt{\alpha_k}\hat{\mathbf{v}}_{m,k}^{\mathrm{H}}\mathbf{w}_m^{P}\right|^2}{\left|\sum_{m=1}^{M}\left(\tilde{\mathbf{h}}_m+\sum_{k=1}^{K}\sqrt{\alpha_k}\tilde{\mathbf{v}}_{m,k}\right)^{\mathrm{H}}\mathbf{w}_m^{P}\right|^2+\sum_{i>k}^{K}\left|\sum_{m=1}^{M}\sqrt{\alpha_i}\hat{\mathbf{v}}_{m,i}^{\mathrm{H}}\mathbf{w}_m^{P}\right|^2+\sigma^2}. \tag{32}$$

backscatter symbols of BD_k in (32). The sum throughput of BDs during the PSR phase, denoted by R_{sum}^{P}, is expressed as

$$R_{\text{sum}}^{P}=t_2 B\mathbb{E}_{\tilde{\mathbf{h}}_m,\tilde{\mathbf{v}}_{m,k}}\left[\log_2(1+\gamma_{\text{sum}}^{P})\right], \tag{33}$$

where γ_{sum}^{P} denotes the accumulated SINR of the receiver decoding the backscatter symbols of the BDs as

$$\gamma_{\text{sum}}^{P}=\frac{\vartheta\sum_{k=1}^{K}\left|\sum_{m=1}^{M}\sqrt{\alpha_k}\hat{\mathbf{v}}_{m,k}^{\mathrm{H}}\mathbf{w}_m^{P}\right|^2}{\left|\sum_{m=1}^{M}\left(\tilde{\mathbf{h}}_m+\sum_{k=1}^{K}\sqrt{\alpha_k}\tilde{\mathbf{v}}_{m,k}\right)^{\mathrm{H}}\mathbf{w}_m^{P}\right|^2+\sigma^2}. \tag{34}$$

Based on (20) and (28), the sum throughput of APs during one time slot, denoted by R_{sum}, is expressed as

$$R_{\text{sum}}=R^{C}+R^{P}. \tag{35}$$

Based on (13), (26), and (33), the sum throughput of BDs during one time slot, denoted by $R_{b,\text{sum}}$, is expressed as

$$R_{b,\text{sum}}=R_{\text{sum}}^{C}+R_{\text{sum}}^{P}+R_{\text{sum}}^{A}. \tag{36}$$

For readability, R_{sum} is referred to as the sum primary throughput, and $R_{b,\text{sum}}$ is referred to as the sum backscatter throughput.

III. Problem Formulation and Analysis

We formulate the sum backscatter throughput maximization problem with the minimum sum primary throughput constraint by jointly optimizing time allocation vector $\boldsymbol{t}$, beamforming vectors $\mathbf{w}^{C}$, $\mathbf{w}^{P}$, and $\mathbf{w}^{A}$, and reflection coefficients $\boldsymbol{\alpha}$ as

$$\begin{aligned}
\mathbf{P0}: \max_{\boldsymbol{t},\mathbf{w}^{C},\mathbf{w}^{P},\mathbf{w}^{A},\boldsymbol{\alpha}} \quad & R_{b,\text{sum}} && \text{(37a)}\\
s.t. \quad & R_{\text{sum}}\geq R_{\min}, && \text{(37b)}\\
& \left\|\mathbf{w}_m^{C}\right\|^2\leq P_m,\forall m\in\mathcal{M}, && \text{(37c)}\\
& \left\|\mathbf{w}_m^{P}\right\|^2\leq P_m,\forall m\in\mathcal{M}, && \text{(37d)}\\
& t_1 P_{\text{cir,C}}^{B}+t_2 P_{\text{cir,P}}^{B}+t_3(P_{\text{cir}}^{A}+\left\|\mathbf{w}_k^{A}\right\|^2)\\
& \leq E_k^{\text{total}},\forall k\in\mathcal{K}, && \text{(37e)}\\
& 0\leq\alpha_k\leq 1,\forall k\in\mathcal{K}, && \text{(37f)}\\
& t_1+t_2+t_3\leq T, t_1,t_2,t_3\geq 0, && \text{(37g)}
\end{aligned}$$

where $\boldsymbol{t}=[t_1,t_2,t_3]$, $\mathbf{w}^{C}=[(\mathbf{w}_1^{C})^{\mathrm{H}},\ldots,(\mathbf{w}_M^{C})^{\mathrm{H}}]^{\mathrm{H}}$ represents the beamforming vector of APs during the CSR phase, $\mathbf{w}^{P}=[(\mathbf{w}_1^{P})^{\mathrm{H}},\ldots,(\mathbf{w}_M^{P})^{\mathrm{H}}]^{\mathrm{H}}$ represents the beamforming vector of APs during the PSR phase, $\mathbf{w}^{A}=[(\mathbf{w}_1^{A})^{\mathrm{H}},\ldots,(\mathbf{w}_K^{A})^{\mathrm{H}}]^{\mathrm{H}}$ represents the beamforming vector of BDs during the AC phase, and $\boldsymbol{\alpha}=[\alpha_1,\ldots,\alpha_K]$ represents the reflection coefficients of BDs. $R_{\min}$ denotes the minimum sum primary throughput, P_m denotes the maximum transmit power of AP_m, $P_{\text{cir,C}}^{B}$ denotes the circuit power for backscatter communication of BDs during the CSR phase, $P_{\text{cir,P}}^{B}$ denotes the circuit power for backscatter communication of BDs during the PSR phase, and P_{cir}^{A} denotes the circuit power for AC of BDs during the AC phase. (37b) represents the minimum sum primary throughput constraint, (37c) and (37d) represent the transmit power constraints, (37e) represents the energy consumption constraint of BDs, (37f) and (37g) represent the value ranges of $\boldsymbol{\alpha}$ and $\boldsymbol{t}$, respectively.

To maximize the sum backscatter throughput $R_{b,\text{sum}}$ in (37a), we obtain closed-form expressions of R_{sum} and $R_{b,\text{sum}}$ by taking the expectations of $\tilde{\mathbf{h}}_m$ and $\tilde{\mathbf{v}}_{m,k}$ in (20), (21), and (26), which is challenging since both $\tilde{\mathbf{h}}_m$ and $\tilde{\mathbf{v}}_{m,k}$ are high-dimensional random variables in the logarithmic function. To simplify the expectation operations of $\tilde{\mathbf{h}}_m$ and $\tilde{\mathbf{v}}_{m,k}$, we interchange the order of expectation and logarithm operations for $\tilde{\mathbf{h}}_m$ and $\tilde{\mathbf{v}}_{m,k}$, i.e., taking the expectations of $\tilde{\mathbf{h}}_m$ and $\tilde{\mathbf{v}}_{m,k}$ in the logarithmic function in (20), (21), and (26), and then performing the logarithm operation on $\tilde{\mathbf{h}}_m$ and $\tilde{\mathbf{v}}_{m,k}$. By interchanging the order of expectation and logarithm operations, we obtain lower bounds of R_{sum} and $R_{b,\text{sum}}$ via Jensen's inequality as follows.

According to (22) and (26), the interference caused by CE errors during the CSR phase, denoted by ER^{C}, is

$$\mathrm{ER}^{C}=\left|\sum_{m=1}^{M}\left(\tilde{\mathbf{h}}_m+\sum_{k=1}^{K}\sqrt{\alpha_k}\tilde{\mathbf{v}}_{m,k}\right)^{\mathrm{H}}\mathbf{w}_m^{C}\right|^2. \tag{38}$$

According to (28) and (33), the interference caused by CE

$$\bar{R}_{\text{sum}} = \frac{t_1 B}{p^K} \sum_{\mathbf{c}\in\mathcal{C}} \log_2\left(1 + \frac{\left|\sum_{m=1}^{M}\left(\hat{\mathbf{h}}_m + \sum_{k=1}^{K}\sqrt{\alpha_k}c_k\hat{\mathbf{v}}_{m,k}\right)^{\mathrm{H}}\mathbf{w}_m^C\right|^2}{\sum_{m=1}^{M}(\mathbf{w}_m^C)^{\mathrm{H}}\left(\mathbf{C}_m + \sum_{k=1}^{K}\alpha_k c_k \mathbf{C}_{m,k}\right)\mathbf{w}_m^C + \sigma^2}\right) + t_2 B \log_2\left(1 + \frac{\left|\sum_{m=1}^{M}\hat{\mathbf{h}}_m^{\mathrm{H}}\mathbf{w}_m^P\right|^2}{\sum_{m=1}^{M}(\mathbf{w}_m^P)^{\mathrm{H}}\left(\mathbf{C}_m + \sum_{k=1}^{K}\alpha_k\mathbf{C}_{m,k}\right)\mathbf{w}_m^P + \sum_{k=1}^{K}\left|\sum_{m=1}^{M}\sqrt{\alpha_k}\hat{\mathbf{v}}_{m,k}^{\mathrm{H}}\mathbf{w}_m^P\right|^2 + \sigma^2}\right). \tag{41}$$

$$\bar{R}_{b,\text{sum}} = \frac{t_1 B}{N}\log_2\left(1 + \frac{\vartheta N\sum_{k=1}^{K}\left|\sum_{m=1}^{M}\sqrt{\alpha_k}\hat{\mathbf{v}}_{m,k}^{\mathrm{H}}\mathbf{w}_m^C\right|^2}{N\sum_{m=1}^{M}(\mathbf{w}_m^C)^{\mathrm{H}}\left(\mathbf{C}_m + \sum_{k=1}^{K}\alpha_k\mathbf{C}_{m,k}\right)\mathbf{w}_m^C + \sigma^2}\right) + t_2 B\log_2\left(1 + \frac{\vartheta\sum_{k=1}^{K}\left|\sum_{m=1}^{M}\sqrt{\alpha_k}\hat{\mathbf{v}}_{m,k}^{\mathrm{H}}\mathbf{w}_m^P\right|^2}{\sum_{m=1}^{M}(\mathbf{w}_m^P)^{\mathrm{H}}\left(\mathbf{C}_m + \sum_{k=1}^{K}\alpha_k\mathbf{C}_{m,k}\right)\mathbf{w}_m^P + \sigma^2}\right) + t_3 B\log_2\left(1 + \frac{\sum_{k=1}^{K}\left|\mathbf{g}_k^{\mathrm{H}}\mathbf{w}_k^A\right|^2}{\sigma^2}\right). \tag{42}$$

errors during the PSR phase, denoted by ER^P, is

$$\mathrm{ER}^P = \left|\sum_{m=1}^{M}\left(\tilde{\mathbf{h}}_m + \sum_{k=1}^{K}\sqrt{\alpha_k}\tilde{\mathbf{v}}_{m,k}\right)^{\mathrm{H}}\mathbf{w}_m^P\right|^2. \tag{39}$$

It is easy to observe that $\mathrm{ER}^C + \sigma^2 > 0$ and $\mathrm{ER}^P + \sigma^2 > 0$ hold. Then according to (20), (21), and (26), $R_{b,\text{sum}}$ and R_{sum} are convex functions of $\tilde{\mathbf{h}}_m$ and $\tilde{\mathbf{v}}_{m,k}$ due to the fact that $\log(1+\frac{C}{x})$ is a convex function of x when $x > 0$ holds. Jensen's inequality shows that $\mathbb{E}[f(x)] \geq f(\mathbb{E}[x])$ holds when $f(x)$ is a convex function. By applying Jensen's inequality to (35) and (36), we obtain the lower bound of $R_{b,\text{sum}}$, denoted by $\bar{R}_{b,\text{sum}}$, the lower bound of R_{sum}, denoted by $\bar{R}_{\text{sum}}$, and derive $\mathbb{E}_{\tilde{\mathbf{h}}_m,\tilde{\mathbf{v}}_{m,k}}[\mathrm{ER}^C]$ and $\mathbb{E}_{\hat{\mathbf{h}}_m,\hat{\mathbf{v}}_{m,k}}[\mathrm{ER}^P]$ in Lemma 1.

Lemma 1: Given $\tilde{\mathbf{h}}_m \sim \mathcal{CN}(0,\mathbf{C}_m)$ and $\tilde{\mathbf{v}}_{m,k} \sim \mathcal{CN}(0,\mathbf{C}_{m,k})$, we obtain

$$\mathbb{E}_{\tilde{\mathbf{h}}_m,\tilde{\mathbf{v}}_{m,k}}[\mathrm{ER}^X] = \sum_{m=1}^{M}(\mathbf{w}_m^X)^{\mathrm{H}}\Big(\mathbf{C}_m + \sum_{k=1}^{K}\alpha_k\mathbf{C}_{m,k}\Big)\mathbf{w}_m^X, \quad \forall X\in\{C,P\}. \tag{40}$$

Proof: Please refer to Appendix A. ∎

According to Lemma 1, we obtain the closed-form expression of $\bar{R}_{\text{sum}}$ in (41) and that of $\bar{R}_{b,\text{sum}}$ in (42).

By taking $\bar{R}_{b,\text{sum}}$ as the optimization objective and $\bar{R}_{\text{sum}}$ as the sum primary throughput, we formulate the sum backscatter throughput maximization problem $\mathbf{P1}$. The minimum sum primary throughput constraint in $\mathbf{P1}$ is stricter than that in $\mathbf{P0}$, thus the optimal solution of $\mathbf{P1}$ is guaranteed to be an approximate optimal solution of $\mathbf{P0}$.

$$\mathbf{P1}: \max_{\boldsymbol{t},\mathbf{w}^C,\mathbf{w}^P,\mathbf{w}^A,\boldsymbol{\alpha}} \bar{R}_{b,\text{sum}} \tag{43a}$$

$$s.t. \quad \bar{R}_{\text{sum}} \geq R_{\min}, \tag{43b}$$

(37b)-(37g).

According to $\bar{R}_{\text{sum}}$ in (41), $\bar{R}_{b,\text{sum}}$ in (42) and E_k^{total} in (11), (37e), (43a), and (43b) are non-convex. Then $\mathbf{P1}$ is a non-convex optimization problem.

IV. BSS Algorithm

To solve $\mathbf{P1}$, we propose the BSS algorithm. As there is no coupling relationship among $\mathbf{w}^C$, $\mathbf{w}^P$, and $\mathbf{w}^A$ in (41) and (42), we decompose $\mathbf{P1}$ into three subproblems, and alternately optimize the TAO subproblem $\mathbf{P2}$, BO subproblem $\mathbf{P3}$, and RCO subproblem $\mathbf{P4}$ by using the BCD method as shown in Fig. 3. We utilize the CVX toolbox to obtain the optimal solution of $\mathbf{P2}$, utilize the SDR method and SCA method to solve $\mathbf{P3}$ and $\mathbf{P4}$. The CPU performs the proposed BSS algorithm to obtain the solution of $\mathbf{P1}$, transmits it to the APs via the fronthaul links, and then the APs broadcast the beamforming vectors, reflection coefficients, and time allocation to the BDs.

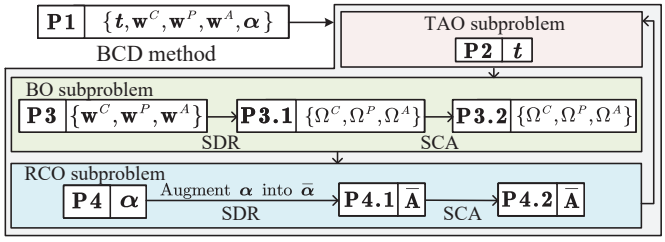

Fig. 3. The flow chart of the proposed BSS algorithm for $\mathbf{P1}$.

A. TAO Subproblem

With given values of $\mathbf{w}^C, \mathbf{w}^P, \mathbf{w}^A$ and $\boldsymbol{\alpha}$ in $\mathbf{P2}$, we optimize $\boldsymbol{t}$ to maximize the sum backscatter throughput as

$$\mathbf{P2}: \max_{\boldsymbol{t}} \quad \bar{R}_{b,\text{sum}} \tag{44a}$$

$$s.t. \quad \bar{R}_{\text{sum}} \geq R_{\min}, \tag{44b}$$

$$t_1 P_{\text{cir,C}}^B + t_2 P_{\text{cir,P}}^B + t_3(P_{\text{cir}}^A + \left\|\mathbf{w}_k^A\right\|^2) \leq E_k^{\text{total}}, \forall k\in\mathcal{K}, \tag{44c}$$

$$t_1 + t_2 + t_3 \leq T, t_1, t_2, t_3 \geq 0. \tag{44d}$$

According to (42), (44b)-(44d), $\mathbf{P2}$ is a LP problem that can be efficiently solved by using the CVX toolbox.

B. BO Subproblem

With given values of $\boldsymbol{t}$ and $\boldsymbol{\alpha}$ in $\mathbf{P3}$, we optimize $\mathbf{w}^C, \mathbf{w}^P$, and $\mathbf{w}^A$ to maximize $\bar{R}_{b,\text{sum}}$ as

$$\mathbf{P3}: \max_{\mathbf{w}^C,\mathbf{w}^P,\mathbf{w}^A} \bar{R}_{b,\text{sum}} \tag{45a}$$

$$s.t. \quad \bar{R}_{\text{sum}} \geq R_{\min}, \tag{45b}$$

$$\left\|\mathbf{w}_m^C\right\|^2 \le P_m, \forall m \in \mathcal{M}, \tag{45c}$$

$$\left\|\mathbf{w}_m^P\right\|^2 \le P_m, \forall m \in \mathcal{M}, \tag{45d}$$

$$t_1 P_{\text{cir,C}}^B + t_2 P_{\text{cir,P}}^B + t_3(P_{\text{cir}}^A + \left\|\mathbf{w}_k^A\right\|^2) \le E_k^{\text{total}}, \forall k \in \mathcal{K}, \tag{45e}$$

According to the expression of $\bar{R}_{\text{sum}}$ in (41), that of $\bar{R}_{b,\text{sum}}$ in (42), and that of E_k^{total} in (11), (45a), (45b), and (45e) are non-convex. To tackle $\mathbf{P3}$, we convert it into a tractable form by using the semi-definite programming (SDP) method.

To make $\mathbf{P3}$ tractable, we define cascaded vectors as $\hat{\mathbf{v}}_k^{\text{H}} = [\hat{\mathbf{v}}_{1,k}^{\text{H}}, \ldots, \hat{\mathbf{v}}_{M,k}^{\text{H}}]$, $\hat{\mathbf{h}}^{\text{H}} = [\hat{\mathbf{h}}_1^{\text{H}}, \ldots, \hat{\mathbf{h}}_M^{\text{H}}]$, and $\hat{\mathbf{e}}^{\text{H}}(\mathbf{c}) = [\hat{\mathbf{e}}_1^{\text{H}}(\mathbf{c}), \ldots, \hat{\mathbf{e}}_M^{\text{H}}(\mathbf{c})]$, where $\hat{\mathbf{e}}_m(\mathbf{c}) = \hat{\mathbf{h}}_m + \sum_{k=1}^K \sqrt{\alpha_k} c_k \hat{\mathbf{v}}_{m,k}$. By employing the principles of the SDP method [32], we let $\hat{\mathbf{V}}_k = \hat{\mathbf{v}}_k \hat{\mathbf{v}}_k^{\text{H}}$, $\hat{\mathbf{H}} = \hat{\mathbf{h}}\hat{\mathbf{h}}^{\text{H}}$, $\hat{\mathbf{E}}(\mathbf{c}) = \hat{\mathbf{e}}(\mathbf{c})\hat{\mathbf{e}}^{\text{H}}(\mathbf{c})$, and $\mathbf{G}_k = \mathbf{g}_k \mathbf{g}_k^{\text{H}}$. Then we introduce variables $\mathbf{\Omega}^C = \mathbf{w}^C(\mathbf{w}^C)^{\text{H}}$, $\mathbf{\Omega}^P = \mathbf{w}^P(\mathbf{w}^P)^{\text{H}}$, and $\mathbf{\Omega}_k^A = \mathbf{w}_k^A(\mathbf{w}_k^A)^{\text{H}}$. Optimizing $\mathbf{w}^C$, $\mathbf{w}^P$, and $\mathbf{w}_k^A$ in $\mathbf{P3}$ is equivalent to optimizing $\mathbf{\Omega}^C$, $\mathbf{\Omega}^P$, and $\mathbf{\Omega}_k^A$ when $\mathbf{\Omega}^C$, $\mathbf{\Omega}^P$, and $\mathbf{\Omega}_k^A$ satisfy properties of positive semi-definite and rank-one, e.g., $\mathbf{\Omega}^C \succeq 0$ and $\text{Rank}(\mathbf{\Omega}^C) = 1$. Detailed conversion procedure about (45a), (45b), and (45e) is provided as follows.

First, we equivalently convert (45a) into a convex function by using the SDP method to tackle the terms that result in non-convexity in (42). According to the first and second terms on the right hand side of the equality in (42), we have

$$\sum_{k=1}^K \left|\sum_{m=1}^M \sqrt{\alpha_k} \hat{\mathbf{v}}_{m,k}^{\text{H}} \mathbf{w}_m^X\right|^2 = \sum_{k=1}^K \alpha_k \left|\hat{\mathbf{v}}_k^{\text{H}} \mathbf{w}^X\right|^2 = \sum_{k=1}^K \alpha_k \text{Tr}(\hat{\mathbf{V}}_k \Omega^X), \forall X \in \{C,P\}, \tag{46}$$

$$\sum_{m=1}^M (\mathbf{w}_m^X)^{\text{H}} \Big(\mathbf{C}_m + \sum_{k=1}^K \alpha_k \mathbf{C}_{m,k}\Big) \mathbf{w}_m^X = \text{Tr}(\mathbf{\Lambda}\mathbf{\Omega}^X), \quad \forall X \in \{C,P\}, \tag{47}$$

where $\mathbf{\Lambda} = \text{Diag}(\aleph_1, \ldots, \aleph_M) \in \mathbb{C}^{MQ \times MQ}$ is a block diagonal matrix, and $\aleph_m = \mathbf{C}_m + \sum_{k=1}^K \alpha_k \mathbf{C}_{m,k}$ holds. According to the third term on the right hand side of the equality in (42), we have

$$\sum_{k=1}^K \left|\mathbf{g}_k^H \mathbf{w}_k^A\right|^2 = \sum_{k=1}^K (\mathbf{w}_k^A)^{\text{H}} \mathbf{g}_k \mathbf{g}_k^{\text{H}} \mathbf{w}_k^A = \sum_{k=1}^K \text{Tr}(\mathbf{G}_k \mathbf{\Omega}_k^A). \tag{48}$$

Second, similar to (46)-(48), we use SDP method to tackle the terms that result in non-convexity in (41). Based on the first term on the right hand side of equality in (41), we have

$$\Big|\sum_{m=1}^M \Big(\hat{\mathbf{h}}_m + \sum_{k=1}^K \sqrt{\alpha_k} c_k \hat{\mathbf{v}}_{m,k}\Big)^{\text{H}} \mathbf{w}_m^C\Big|^2 = \left|\hat{\mathbf{e}}^{\text{H}}(\mathbf{c})\mathbf{w}^C\right|^2 = (\mathbf{w}^C)^{\text{H}} \hat{\mathbf{e}}(\mathbf{c}) \hat{\mathbf{e}}^{\text{H}}(\mathbf{c}) \mathbf{w}^C = \text{Tr}(\hat{\mathbf{E}}(\mathbf{c}) \mathbf{\Omega}^C), \tag{49}$$

$$\sum_{m=1}^M (\mathbf{w}_m^C)^{\text{H}} \Big(\mathbf{C}_m + \sum_{k=1}^K \alpha_k c_k \mathbf{C}_{m,k}\Big) \mathbf{w}_m^C = \text{Tr}(\mathbf{\Lambda}(\mathbf{c}) \mathbf{\Omega}^C), \tag{50}$$

where $\mathbf{\Lambda}(\mathbf{c}) = \text{Diag}(\aleph_1(\mathbf{c}), \ldots, \aleph_M(\mathbf{c})) \in \mathbb{C}^{MQ \times MQ}$, and $\aleph_m(\mathbf{c}) = \mathbf{C}_m + \sum_{k=1}^K \alpha_k c_k \mathbf{C}_{m,k}$.

(45e) is non-convex due to accumulated quadratic terms of $\mathbf{w}_m^C$ in (7), $\mathbf{w}_m^P$ in (10), and $\mathbf{w}_k^A$ in (45e). Then we have the following conversion procedure about (45e), and introduce a block diagonal matrix $\mathbf{F}_k = \text{Diag}(\mathbf{F}_{1,k}, \ldots, \mathbf{F}_{M,k})$. By using the SDP method, we express E_k^{total} in (37e) as

$$\begin{aligned} E_k^{\text{total}} &= \eta(1-\alpha_k)\Big(t_1 \Big\|\sum_{m=1}^M \mathbf{F}_{m,k} \mathbf{w}_m^C\Big\|^2 + t_2 \Big\|\sum_{m=1}^M \mathbf{F}_{m,k} \mathbf{w}_m^P\Big\|^2\Big) \\ &= \eta(1-\alpha_k)\big(t_1 \text{Tr}(\mathbf{F}_k \mathbf{\Omega}^C \mathbf{F}_k^{\text{H}}) + t_2 \text{Tr}(\mathbf{F}_k \mathbf{\Omega}^P \mathbf{F}_k^{\text{H}})\big). \end{aligned} \tag{51}$$

Based on (46)-(51), $\mathbf{P3}$ can be equivalently formulated as

$\mathbf{P3.1}$:

$$\begin{aligned} \max_{\mathbf{\Omega}^C, \mathbf{\Omega}^P, \mathbf{\Omega}^A} \; & \frac{t_1 B}{N} \log_2\Big(1 + \frac{\vartheta N \sum_{k=1}^K \alpha_k \text{Tr}(\hat{\mathbf{V}}_k \mathbf{\Omega}^C)}{N \text{Tr}(\mathbf{\Lambda}\mathbf{\Omega}^C) + \sigma^2}\Big) \\ & + t_2 B \log_2\Big(1 + \frac{\vartheta \sum_{k=1}^K \alpha_k \text{Tr}(\hat{\mathbf{V}}_k \mathbf{\Omega}^P)}{\text{Tr}(\mathbf{\Lambda}\mathbf{\Omega}^P) + \sigma^2}\Big) \\ & + t_3 B \log_2\Big(1 + \frac{\sum_{k=1}^K \text{Tr}(\mathbf{G}_k \mathbf{\Omega}_k^A)}{\sigma^2}\Big) \end{aligned} \tag{52a}$$

$$s.t. \quad t_2 B \log_2\Big(1 + \frac{\text{Tr}(\hat{\mathbf{H}}\mathbf{\Omega}^P)}{\text{Tr}(\mathbf{\Lambda}\mathbf{\Omega}^P) + \sum_{k=1}^K \alpha_k \text{Tr}(\hat{\mathbf{V}}_k \mathbf{\Omega}^P) + \sigma^2}\Big) + \frac{t_1 B}{p^M} \sum_{i=1}^{p^M} \log_2\Big(1 + \frac{\text{Tr}(\hat{\mathbf{E}}(\mathbf{c})\mathbf{\Omega}^C)}{\text{Tr}(\mathbf{\Lambda}(\mathbf{c})\mathbf{\Omega}^C) + \sigma^2}\Big) \ge R_{\min}, \tag{52b}$$

$$\text{Tr}(\mathbf{\Omega}^X[(m-1)Q+1 : mQ]) \le P_m, \quad \forall m \in \mathcal{M}, \forall X \in \{C,P\}, \tag{52c}$$

$$t_1 P_{\text{cir,C}}^B + t_2 P_{\text{cir,P}}^B + t_3(P_{\text{cir}}^A + \text{Tr}(\mathbf{\Omega}_k^A)) \le E_k^{\text{total}}, \forall k \in \mathcal{K}, \tag{52d}$$

$$\mathbf{\Omega}^X \succeq 0, \forall X \in \{C,P\}, \tag{52e}$$

$$\mathbf{\Omega}_k^A \succeq 0, \forall k \in \mathcal{K}, \tag{52f}$$

$$\text{Rank}(\mathbf{\Omega}^X) = 1, \forall X \in \{C,P\}, \tag{52g}$$

$$\text{Rank}(\mathbf{\Omega}_k^A) = 1, \forall k \in \mathcal{K}. \tag{52h}$$

Specifically, $\mathbf{a}[m : m+n]$ represents the submatrix of $\mathbf{a}$ made up of its m-th row and m-th column to $(m+n)$-th row and $(m+n)$-th column elements.

$\mathbf{P3.1}$ is a non-convex problem due to the fractional structure of $\mathbf{\Omega}^C$ and $\mathbf{\Omega}^P$ in (52a) and (52b), and rank-one constraints in (52g) and (52h). To address $\mathbf{P3.1}$, we adopt the SCA method [34] to optimize the objective function in (52a) iteratively. Let $(\mathbf{\Omega}^{C(l)}, \mathbf{\Omega}^{P(l)}, \mathbf{\Omega}_k^{A(l)}), \forall k \in \mathcal{K}$ denote a local solution of $\mathbf{P3.1}$ at the l-th iteration. The first-order Taylor series provides a linear convex approximation of the non-convex function, and is used to approximate the terms that result in non-convexity in (52a) and (52b) as

$$\log_2\big(\text{Tr}(\mathbf{\Lambda}\mathbf{\Omega}^X) + \sigma^2\big) \le \log_2\big(\text{Tr}(\mathbf{\Lambda}\mathbf{\Omega}^{X(l)}) + \sigma^2\big) + \frac{\text{Tr}(\mathbf{\Lambda}\mathbf{\Omega}^X) + \sigma^2}{(\text{Tr}(\mathbf{\Lambda}\mathbf{\Omega}^{X(l)}) + \sigma^2)\ln 2} + \frac{1}{\ln 2}, \quad \forall X \in \{C,P\}, \tag{53}$$

$$\log_2\big(\text{Tr}(\mathbf{\Lambda}\mathbf{\Omega}^P) + \sum_{k=1}^K \alpha_k \text{Tr}(\hat{\mathbf{V}}_k \mathbf{\Omega}^P) + \sigma^2\big) \le \log_2\big(\text{Tr}(\mathbf{\Lambda}\mathbf{\Omega}^{P(l)}) + \sum_{k=1}^K \alpha_k \text{Tr}(\hat{\mathbf{V}}_k \mathbf{\Omega}^{P(l)}) + \sigma^2\big)$$

$$\mathbf{P3.2}: \max_{\mathbf{\Omega}^C,\mathbf{\Omega}^P,\mathbf{\Omega}^A} \frac{t_1 B}{N}\Big(\log_2\Big(\frac{N\mathrm{Tr}(\mathbf{\Lambda}\mathbf{\Omega}^C)+\vartheta N\sum_{k=1}^K \alpha_k \mathrm{Tr}(\hat{\mathbf{V}}_k\mathbf{\Omega}^C)+\sigma^2}{N\mathrm{Tr}(\mathbf{\Lambda}\mathbf{\Omega}^{C(l)})+\sigma^2}\Big)-\frac{N\mathrm{Tr}(\mathbf{\Lambda}\mathbf{\Omega}^C)+\sigma^2}{(N\mathrm{Tr}(\mathbf{\Lambda}\mathbf{\Omega}^{C(l)})+\sigma^2)\ln 2}+\frac{1}{\ln 2}\Big)$$
$$+t_2 B\Big(\log_2\Big(\frac{\mathrm{Tr}(\mathbf{\Lambda}\mathbf{\Omega}^P)+\vartheta\sum_{k=1}^K \alpha_k \mathrm{Tr}(\hat{\mathbf{V}}_k\mathbf{\Omega}^P)+\sigma^2}{\mathrm{Tr}(\mathbf{\Lambda}\mathbf{\Omega}^{P(l)})+\sigma^2}\Big)-\frac{\mathrm{Tr}(\mathbf{\Lambda}\mathbf{\Omega}^P)+\sigma^2}{(\mathrm{Tr}(\mathbf{\Lambda}\mathbf{\Omega}^{P(l)})+\sigma^2)\ln 2}+\frac{1}{\ln 2}\Big)$$
$$+t_3 B\log_2\Big(1+\frac{\sum_{k=1}^K \mathrm{Tr}(\mathbf{G}_k\mathbf{\Omega}_k^A)}{\sigma^2}\Big) \tag{55a}$$
$$s.t. \quad \frac{t_1 B}{p^M}\sum_{i=1}^{p^M}\Big(\log_2\Big(\frac{\mathrm{Tr}(\mathbf{\Lambda}(\mathbf{c})\mathbf{\Omega}^C)+\mathrm{Tr}(\hat{\mathbf{E}}(\mathbf{c})\mathbf{\Omega}^C)+\sigma^2}{\mathrm{Tr}(\mathbf{\Lambda}(\mathbf{c})\mathbf{\Omega}^{C(l)})+\sigma^2}\Big)-\frac{\mathrm{Tr}(\mathbf{\Lambda}(\mathbf{c})\mathbf{\Omega}^C)+\sigma^2}{(\mathrm{Tr}(\mathbf{\Lambda}(\mathbf{c})\mathbf{\Omega}^{C(l)})+\sigma^2)\ln 2}+\frac{1}{\ln 2}\Big)$$
$$+t_2 B\Big(\log_2\Big(\frac{\mathrm{Tr}(\hat{\mathbf{H}}\mathbf{\Omega}^P)+\mathrm{Tr}(\mathbf{\Lambda}\mathbf{\Omega}^P)+\sum_{k=1}^K \alpha_k \mathrm{Tr}(\hat{\mathbf{V}}_k\mathbf{\Omega}^P)+\sigma^2}{\mathrm{Tr}(\mathbf{\Lambda}\mathbf{\Omega}^{P(l)})+\sum_{k=1}^K \alpha_k \mathrm{Tr}(\hat{\mathbf{V}}_k\mathbf{\Omega}^{P(l)})+\sigma^2}\Big)$$
$$-\frac{\mathrm{Tr}(\mathbf{\Lambda}\mathbf{\Omega}^P)+\sum_{k=1}^K \alpha_k \mathrm{Tr}(\hat{\mathbf{V}}_k\mathbf{\Omega}^P)+\sigma^2}{(\mathrm{Tr}(\mathbf{\Lambda}\mathbf{\Omega}^{P(l)})+\sum_{k=1}^K \alpha_k \mathrm{Tr}(\hat{\mathbf{V}}_k\mathbf{\Omega}^{P(l)})+\sigma^2)\ln 2}+\frac{1}{\ln 2}\Big)\geq R_{\min}, \tag{55b}$$
(52c)-(52h).

Algorithm 1 BO Algorithm for $\mathbf{P3}$

Input: The maximum iteration number $I_{\max}$, preset error precision ϵ, $\boldsymbol{t}$, $\boldsymbol{\alpha}$, P_m, and $R_{\min}$.
Output: $(\mathbf{w}^{C(*)},\mathbf{w}^{P(*)},\mathbf{w}^{A(*)})$ of $\mathbf{P3}$.
1: Initialization: Set iteration number $l=0$, and initial solution $\mathbf{\Phi}^{(0)}=(\mathbf{\Omega}^{C(0)},\mathbf{\Omega}^{P(0)},\mathbf{\Omega}^{A(0)})$.
2: **repeat**
3: Solve $\mathbf{P3.2}$ with given $\mathbf{\Phi}^{(l)}=(\mathbf{\Omega}^{C(l)},\mathbf{\Omega}^{P(l)},\mathbf{\Omega}^{A(l)})$, and obtain the approximate optimal solution of $\mathbf{P3.2}$ at the l-th iteration $\mathbf{\Phi}^{(*l)}=(\mathbf{\Omega}^{C(*l)},\mathbf{\Omega}^{P(*l)},\mathbf{\Omega}^{A(*l)})$.
4: Calculate $\bar{R}_{b,\text{sum}}^{(l)}$ under $\mathbf{\Phi}^{(*l)}$ in (52a).
5: Update $\mathbf{\Phi}^{(l+1)}=\mathbf{\Phi}^{(*l)}$ and $l=l+1$.
6: **until** $l>I_{\max}$ or $\big|\bar{R}_{b,\text{sum}}^{(l+1)}-\bar{R}_{b,\text{sum}}^{(l)}\big|\leq\epsilon$.
7: Exploit Gaussian randomization to obtain the output.

$$+\frac{\mathrm{Tr}(\mathbf{\Lambda}\mathbf{\Omega}^P)+\sum_{k=1}^K \alpha_k \mathrm{Tr}(\hat{\mathbf{V}}_k\mathbf{\Omega}^P)+\sigma^2}{(\mathrm{Tr}(\mathbf{\Lambda}\mathbf{\Omega}^{P(l)})+\sum_{k=1}^K \alpha_k \mathrm{Tr}(\hat{\mathbf{V}}_k\mathbf{\Omega}^{P(l)})+\sigma^2)\ln 2}+\frac{1}{\ln 2}. \tag{54}$$

According to (53) and (54), $\mathbf{P3.1}$ is transformed as $\mathbf{P3.2}$.

For given local solution $(\mathbf{\Omega}^{C(l)},\mathbf{\Omega}^{P(l)},\mathbf{\Omega}_k^{A(l)}),\forall k\in\mathcal{K}$, (55a), (55b), and (52c)-(52f) are convex. $\mathbf{P3.2}$ is non-convex due to rank-one constraints (52g) and (52h). According to the SDR method, we further relax (52g) and (52h) by omitting them, and solve $\mathbf{P3.2}$ by using the CVX toolbox. Algorithm 1 summarizes the optimization of $(\mathbf{w}^C,\mathbf{w}^P,\mathbf{w}^A)$ in $\mathbf{P3}$.

Remark 1: By using the SCA method, an approximate optimal solution $(\mathbf{\Omega}^{C(*)},\mathbf{\Omega}^{P(*)},\mathbf{\Omega}^{A(*)})$ of $\mathbf{P3.1}$ can be obtained when $\mathbf{P3.2}$ iteratively converges. If $\mathbf{\Omega}^{C(*)},\mathbf{\Omega}^{P(*)}$, and $\mathbf{\Omega}^{A(*)}$ are rank-one, $(\mathbf{\Omega}^{C(*)},\mathbf{\Omega}^{P(*)},\mathbf{\Omega}^{A(*)})$ can be equivalently transformed into an approximate optimal solution $(\mathbf{w}^{C(*)},\mathbf{w}^{P(*)},\mathbf{w}^{A(*)})$ of $\mathbf{P3}$ by using eigenvalue decomposition. However, the SDR method does not always obtain the rank-one beamforming matrix [35]. For the case that the rank of beamforming matrix is larger than one, existing methods, such as the difference-of-convex algorithm and Gaussian randomization [36], can be used to obtain an approximate optimal solution. According to [35], the Gaussian randomization achieves a $\frac{\pi}{4}$-approximation of the optimal solution, and we use the Gaussian randomization to obtain an approximate optimal solution of $\mathbf{P3}$ in Algorithm 1.

C. RCO Subproblem

With given values of $\boldsymbol{t}$, $\mathbf{w}^C$, $\mathbf{w}^P$, and $\mathbf{w}^A$ in $\mathbf{P4}$, we optimize $\boldsymbol{\alpha}$ to maximize $\bar{R}_{b,\text{sum}}$ as

$$\mathbf{P4}: \max_{\boldsymbol{\alpha}} \quad \bar{R}_{b,\text{sum}} \tag{56a}$$
$$s.t. \quad \bar{R}_{\text{sum}}\geq R_{\min}, \tag{56b}$$
$$t_1 P_{\text{cir,C}}^B + t_2 P_{\text{cir,P}}^B + t_3(P_{\text{cir}}^A+\big\|\mathbf{w}_k^A\big\|^2)$$
$$\leq E_k^{\text{total}},\forall k\in\mathcal{K}, \tag{56c}$$
$$0\leq\alpha_k\leq 1,\forall k\in\mathcal{K}. \tag{56d}$$

According to the expression of $\bar{R}_{\text{sum}}$ in (41) and that of $\bar{R}_{b,\text{sum}}$ in (42), (56a) and (56b) are non-convex. Similar to the conversion procedure of $\mathbf{P3}$, we convert $\mathbf{P4}$ into a tractable form by using the SDP method as follows. We equivalently convert (56b) into a convex constraint, and tackle the terms that result in non-convexity in (41). According to the first term on the right hand side of the equality in (41), we have

$$\Big|\sum_{m=1}^M\big(\hat{\mathbf{h}}_m+\sum_{k=1}^K\sqrt{\alpha_k}c_k\hat{\mathbf{v}}_{m,k}\big)^{\mathrm{H}}\mathbf{w}_m^C\Big|^2$$
$$=\big|\hat{\mathbf{h}}^{\mathrm{H}}\mathbf{w}^C\big|^2+\bar{\boldsymbol{\alpha}}^{\mathrm{T}}\mathbf{R}\bar{\boldsymbol{\alpha}}=\big|\hat{\mathbf{h}}^{\mathrm{H}}\mathbf{w}^C\big|^2+\mathrm{Tr}(\mathbf{R}\bar{\mathbf{A}}), \tag{57}$$

where $\mathbf{R}=\begin{bmatrix}\mathbf{\Upsilon}\mathbf{\Upsilon}^{\mathrm{H}} & \mathbf{\Upsilon}\hat{\mathbf{h}}^{\mathrm{H}}\mathbf{w}^C\\ \hat{\mathbf{h}}^{\mathrm{H}}\mathbf{w}^C\mathbf{\Upsilon}^{\mathrm{H}} & \mathbf{0}\end{bmatrix}$, $\mathbf{\Upsilon}=\big[c_1\mathbf{v}_1^{\mathrm{H}}\mathbf{w}^C,\ldots,c_K\mathbf{v}_K^{\mathrm{H}}\mathbf{w}^C\big]^{\mathrm{H}}\in\mathbb{C}^{K\times 1}$, $\bar{\boldsymbol{\alpha}}=\begin{bmatrix}\sqrt{\boldsymbol{\alpha}}\\ 1\end{bmatrix}$, and $\bar{\mathbf{A}}=\bar{\boldsymbol{\alpha}}\bar{\boldsymbol{\alpha}}^{\mathrm{T}}$ is the introduced variable. Optimizing $\boldsymbol{\alpha}$ in $\mathbf{P4}$ is equivalent to optimizing $\bar{\mathbf{A}}$ when $\bar{\mathbf{A}}$ satisfies the properties of positive semi-definite and rank-one, i.e., $\bar{\mathbf{A}}\succeq 0$ and $\mathrm{Rank}(\bar{\mathbf{A}})=1$ hold. Based on (41), we have

$$\sum_{m=1}^M(\mathbf{w}_m^C)^{\mathrm{H}}\Big(\mathbf{C}_m+\sum_{k=1}^K\alpha_k c_k\mathbf{C}_{m,k}\Big)\mathbf{w}_m^C+\sigma^2$$
$$=\bar{\boldsymbol{\alpha}}^{\mathrm{T}}\mathbf{\Gamma}^C(\mathbf{c})\bar{\boldsymbol{\alpha}}+T_1=\mathrm{Tr}(\mathbf{\Gamma}^C(\mathbf{c})\bar{\mathbf{A}})+T_1, \tag{58}$$

Algorithm 2 RCO Algorithm for $\mathbf{P4}$

Input: $I_{\max}$, ϵ, $\boldsymbol{t}$, P_m, $R_{\min}$, and $(\mathbf{w}^C, \mathbf{w}^P, \mathbf{w}^A)$.
Output: The approximate optimal solution $\boldsymbol{\alpha}^{(*)}$ of $\mathbf{P4}$.
1: Initialization: Set iteration number $l = 0$, and initial solution $\bar{\mathbf{A}}^{(0)}$.
2: **repeat**
3: Solve $\mathbf{P4.2}$ with given $\bar{\mathbf{A}}^{(l)}$, and obtain the approximate optimal solution of $\mathbf{P4.2}$ at the l-th iteration $\bar{\mathbf{A}}^{(*l)}$.
4: Calculate $\bar{R}_{b,\text{sum}}^{(l)}$ under $\bar{\mathbf{A}}^{(*l)}$ in (61a).
5: Update $\bar{\mathbf{A}}^{(l+1)} = \bar{\mathbf{A}}^{(*l)}$ and $l = l + 1$.
6: **until** $l > I_{\max}$ or $\left|\bar{R}_{b,\text{sum}}^{(l+1)} - \bar{R}_{b,\text{sum}}^{(l)}\right| \leq \epsilon$.
7: Exploit Gaussian randomization to obtain the corresponding rank-one vector $\bar{\boldsymbol{\alpha}}^{(*)}$.
8: Take the first K elements of $\bar{\boldsymbol{\alpha}}^{(*)}$ as the output.

where $T_1 = N\sum_{m=1}^{M}\left(\mathbf{w}_m^C\right)^{\mathrm{H}}\mathbf{C}_m\mathbf{w}_m^C + \sigma^2$, $\boldsymbol{\Gamma}^X(\mathbf{c}) = \mathrm{Diag}(\mathbf{c}\mathbf{c}^{\mathrm{T}})\boldsymbol{\Gamma}^X$, $\boldsymbol{\Gamma}^X = \mathrm{Diag}\left(\zeta_1^X, \ldots, \zeta_K^X, 0\right) \in \mathbb{C}^{(K+1)\times(K+1)}$, and $\zeta_k^X = \sum_{m=1}^{M}(\mathbf{w}_m^X)^{\mathrm{H}}\mathbf{C}_{m,k}\mathbf{w}_m^X, \quad \forall X \in \{C,P\}$. According to the second term on the right hand side of the equality in (41), we have

$$\Big|\sum_{m=1}^{M}\sqrt{\alpha_k}\hat{\mathbf{v}}_{m,k}^{\mathrm{H}}\mathbf{w}_m^P\Big|^2 = \bar{\boldsymbol{\alpha}}^{\mathrm{T}}\boldsymbol{\Xi}^P\bar{\boldsymbol{\alpha}} = \mathrm{Tr}(\boldsymbol{\Xi}^P\bar{\mathbf{A}}), \tag{59}$$

$$\sum_{m=1}^{M}(\mathbf{w}_m^P)^{\mathrm{H}}\Big(\mathbf{C}_m + \sum_{k=1}^{K}\alpha_k\mathbf{C}_{m,k}\Big)\mathbf{w}_m^P + \sigma^2 = \bar{\boldsymbol{\alpha}}^{\mathrm{T}}\boldsymbol{\Gamma}^P\bar{\boldsymbol{\alpha}} + T_2 = \mathrm{Tr}(\boldsymbol{\Gamma}^P\bar{\mathbf{A}}) + T_2, \tag{60}$$

where $\boldsymbol{\Xi}^P = \mathrm{Diag}\left(\theta_1^P, \ldots, \theta_K^P, 0\right) \in \mathbb{C}^{(K+1)\times(K+1)}$, $\theta_k^P = (\mathbf{w}^P)^{\mathrm{H}}\hat{\mathbf{V}}_k\mathbf{w}^P$, and $T_2 = \sum_{m=1}^{M}\left(\mathbf{w}_m^P\right)^{\mathrm{H}}\mathbf{C}_m\mathbf{w}_m^P + \sigma^2$.

Similar to (57)-(60), we tackle the accumulated quadratic terms that result in non-convexity in (42), and omit the procedure of converting (56a) into a convex function. Then $\mathbf{P4}$ can be equivalently formulated as

$$\begin{aligned}
\mathbf{P4.1}: \max_{\bar{\mathbf{A}}} \; & \frac{t_1 B}{N}\log_2\Big(1 + \frac{\vartheta N\mathrm{Tr}(\boldsymbol{\Xi}^C\bar{\mathbf{A}})}{N\mathrm{Tr}(\boldsymbol{\Gamma}^C\bar{\mathbf{A}}) + T_1}\Big) \\
& + t_2 B\log_2\Big(1 + \frac{\vartheta\mathrm{Tr}(\boldsymbol{\Xi}^P\bar{\mathbf{A}})}{\mathrm{Tr}(\boldsymbol{\Gamma}^P\bar{\mathbf{A}}) + T_2}\Big) \\
& + Bt_3\log_2\Big(1 + \frac{\sum_{k=1}^{K}\left|\mathbf{g}_k^H\mathbf{w}_k^A\right|^2}{\sigma^2}\Big) && \text{(61a)} \\
s.t. \quad & \frac{t_1 B}{p^M}\sum_{i=1}^{p^M}\log_2\Big(1 + \frac{\left|\hat{\mathbf{h}}^{\mathrm{H}}\mathbf{w}^C\right|^2 + \mathrm{Tr}(\mathbf{R}\bar{\mathbf{A}})}{\mathrm{Tr}(\boldsymbol{\Gamma}(\mathbf{c})^C\bar{\mathbf{A}}) + T_1}\Big) \\
& + t_2 B\log_2\Big(1 + \frac{\left|\hat{\mathbf{h}}^{\mathrm{H}}\mathbf{w}^P\right|^2}{\mathrm{Tr}(\boldsymbol{\Gamma}^P\bar{\mathbf{A}}) + \mathrm{Tr}(\boldsymbol{\Xi}^P\bar{\mathbf{A}}) + T_2}\Big) \\
& \geq R_{\min}, && \text{(61b)} \\
& \bar{\mathbf{A}}(k,k) \leq 1 - \frac{t_1 P_{\text{cir,C}}^B + t_2 P_{\text{cir,P}}^B + t_3(P_{\text{cir}}^A + \left\|\mathbf{w}_k^A\right\|^2)}{T_{3,k}}, \\
& \forall k \in \mathcal{K}, && \text{(61c)} \\
& 0 \leq \bar{\mathbf{A}}(k,k) \leq 1, \forall k \in \mathcal{K}, && \text{(61d)} \\
& \bar{\mathbf{A}}(K+1, K+1) = 1, && \text{(61e)} \\
& \bar{\mathbf{A}} \succeq 0, && \text{(61f)} \\
& \mathrm{Rank}(\bar{\mathbf{A}}) = 1, && \text{(61g)}
\end{aligned}$$

Algorithm 3 BSS Algorithm for $\mathbf{P1}$

Input: $I_{\max}$, ϵ, P_m, and $R_{\min}$.
Output: The approximate optimal solution $\boldsymbol{t}^{(*)}, \mathbf{w}^{C(*)}, \mathbf{w}^{P(*)}, \mathbf{w}^{A(*)}$, and $\boldsymbol{\alpha}^{(*)}$ of $\mathbf{P1}$.
1: **repeat**
2: Given $\mathbf{w}^{C(l)}, \mathbf{w}^{P(l)}, \mathbf{w}^{A(l)}$, and $\boldsymbol{\alpha}^{(l)}$, obtain the optimal solution $\boldsymbol{t}^{(l+1)}$ of $\mathbf{P2}$ by using the CVX toolbox.
3: Given $\boldsymbol{t}^{(l+1)}$ and $\boldsymbol{\alpha}^{(l)}$, obtain the approximate optimal solution $(\mathbf{w}^{C(l+1)}, \mathbf{w}^{P(l+1)}, \mathbf{w}^{A(l+1)})$ of $\mathbf{P3}$ according to $\mathbf{Algorithm\ 1}$.
4: Given $\boldsymbol{t}^{(l+1)}$ and $(\mathbf{w}^{C(l+1)}, \mathbf{w}^{P(l+1)}, \mathbf{w}^{A(l+1)})$, obtain the approximate optimal solution $\boldsymbol{\alpha}^{(l+1)}$ of $\mathbf{P4}$ according to $\mathbf{Algorithm\ 2}$.
5: Calculate $\bar{R}_{b,\text{sum}}^{(l+1)}$ under $\boldsymbol{t}^{(l+1)}$, $\mathbf{w}^{C(l+1)}$, $\mathbf{w}^{P(l+1)}$, $\mathbf{w}^{A(l+1)}$, and $\boldsymbol{\alpha}^{(l+1)}$ in (43a).
6: Update $l = l + 1$.
7: **until** $l > I_{\max}$ or $\left|\bar{R}_{b,\text{sum}}^{(l+1)} - \bar{R}_{b,\text{sum}}^{(l)}\right| \leq \epsilon$.

where

$$T_{3,k} = \eta(t_1\|\sum_{m=1}^{M}\mathbf{F}_{m,k}\mathbf{w}_m^C\|^2 + t_2\|\sum_{m=1}^{M}\mathbf{F}_{m,k}\mathbf{w}_m^P\|^2). \tag{62}$$

(56c) is reformulated as (61c), and $\bar{\mathbf{A}}(k,k)$ denotes the element in the k-th row and k-th column of $\bar{\mathbf{A}}$.

$\mathbf{P4.1}$ is a non-convex problem due to the fractional structure of $\bar{\mathbf{A}}$ in (61a) and (61b), and rank-one constraint in (61g). Similar to (53) and (54), we adopt the SCA method to optimize the objective function in (61a) iteratively, and let $\bar{\mathbf{A}}^{(l)}$ denote a local solution of $\mathbf{P4.1}$ at the l-th iteration. By using the first-order Taylor series, (61a) is approximated as a convex function, and (61b) is approximated as a convex constraint. Similar to $\mathbf{P3.2}$ in Section IV-B, we further relax (61g) by omitting it, and solve $\mathbf{P4.2}$ by using the CVX toolbox. For the case that the rank of the solution for $\mathbf{P4.2}$ is larger than one, we use the Gaussian randomization to obtain an approximate optimal solution according to Remark 1. Algorithm 2 summarizes the optimization of $\boldsymbol{\alpha}$ in $\mathbf{P4}$.

To address the issue of computational complexity in the CF-SRN, the cluster-based scheme can be applied in the CF-SRN with large K, i.e., the BSS algorithm is executed within each cluster, and the alternating optimization scheme can be applied in the CF-SRN with large M, i.e., the BSS algorithm alternately optimizes the sub-beamforming vector of the APs in one subset. The BSS algorithm remains applicable in the CF-SRN with multi-receiver, since the SDR method is applicable to optimize the high-dimensional variables and the SCA method addresses the non-convexity caused by the inter-receiver interference. In the CF-SRN with multi-receiver, the computational complexity and inter-receiver interference management are primary limiting factors of the BSS algorithm, which can be studied in the future work.

D. Convergence Discussions

According to [37], the BSS algorithm is guaranteed to converge if the objective function is monotonically non-decreasing in each iteration. It is obvious that the objective function

$$\mathbf{P4.2}: \max_{\bar{\mathbf{A}}} \quad \frac{t_1 B}{N}\left(\log_2\left(\frac{\vartheta N \mathrm{Tr}(\mathbf{\Xi}^C \bar{\mathbf{A}}) + N\mathrm{Tr}(\mathbf{\Gamma}^C \bar{\mathbf{A}}) + T_1}{N\mathrm{Tr}(\mathbf{\Gamma}^C \bar{\mathbf{A}}^{(l)}) + T_1}\right) - \frac{N\mathrm{Tr}(\mathbf{\Gamma}^C \bar{\mathbf{A}}) + T_1}{(N\mathrm{Tr}(\mathbf{\Gamma}^C \bar{\mathbf{A}}^{(l)}) + T_1)\ln 2} + \frac{1}{\ln 2}\right)$$
$$+ t_2 B\left(\log_2\left(\frac{\vartheta \mathrm{Tr}(\mathbf{\Xi}^P \bar{\mathbf{A}}) + \mathrm{Tr}(\mathbf{\Gamma}^P \bar{\mathbf{A}}) + T_2}{\mathrm{Tr}(\mathbf{\Gamma}^P \bar{\mathbf{A}}^{(l)}) + T_2}\right) - \frac{\mathrm{Tr}(\mathbf{\Gamma}^P \bar{\mathbf{A}}) + T_2}{(\mathrm{Tr}(\mathbf{\Gamma}^P \bar{\mathbf{A}}^{(l)}) + T_2)\ln 2} + \frac{1}{\ln 2}\right)$$
$$+ t_3 B \log_2\left(1 + \frac{\sum_{k=1}^{K} \mathrm{Tr}(\mathbf{G}_k \mathbf{\Omega}_k^A)}{\sigma^2}\right) \tag{63a}$$

$$s.t. \quad \frac{t_1 B}{p^M}\sum_{i=1}^{p^M}\left(\log_2\left(\frac{\left|\hat{\mathbf{h}}^{\mathrm{H}}\mathbf{w}^C\right|^2 + \mathrm{Tr}(\mathbf{R}\bar{\mathbf{A}}) + \mathrm{Tr}(\mathbf{\Gamma}(\mathbf{c})^C \bar{\mathbf{A}}) + T_1}{\mathrm{Tr}(\mathbf{\Gamma}(\mathbf{c})^C \bar{\mathbf{A}})^{(l)} + T_1}\right) - \frac{\mathrm{Tr}(\mathbf{\Gamma}(\mathbf{c})^C \bar{\mathbf{A}}) + T_1}{(\mathrm{Tr}(\mathbf{\Gamma}(\mathbf{c})^C \bar{\mathbf{A}})^{(l)} + T_1)\ln 2} + \frac{1}{\ln 2}\right)$$
$$+ t_2 B\left(\log_2\left(\frac{\left|\hat{\mathbf{h}}^{\mathrm{H}}\mathbf{w}^P\right|^2 + \mathrm{Tr}(\mathbf{\Gamma}^P \bar{\mathbf{A}}) + \mathrm{Tr}(\mathbf{\Xi}^P \bar{\mathbf{A}}) + T_2}{\mathrm{Tr}(\mathbf{\Gamma}^P \bar{\mathbf{A}}^{(l)}) + \mathrm{Tr}(\mathbf{\Xi}^P \bar{\mathbf{A}}^{(l)}) + T_2}\right)$$
$$- \frac{\mathrm{Tr}(\mathbf{\Gamma}^P \bar{\mathbf{A}}) + \mathrm{Tr}(\mathbf{\Xi}^P \bar{\mathbf{A}}) + T_2}{(\mathrm{Tr}(\mathbf{\Gamma}^P \bar{\mathbf{A}}^{(l)}) + \mathrm{Tr}(\mathbf{\Xi}^P \bar{\mathbf{A}}^{(l)}) + T_2)\ln 2} + \frac{1}{\ln 2}\right) \geq R_{\min}, \tag{63b}$$
(61c)-(61g).

$\bar{R}_{b,\mathrm{sum}}$ in $\mathbf{P1}$ is monotonically non-decreasing after solving the TAO subproblem in line 2 of Algorithm 3. The reason is that, the optimal solution of $\mathbf{P2}$ is obtained by solving the convex LP problem. Similarly, it is obvious that the objective function in $\mathbf{P1}$ is monotonically non-decreasing after solving the BO and RCO subproblems in lines 3 and 4 of Algorithm 3, respectively. The reason is that the optimal solutions of $\mathbf{P3.2}$ and $\mathbf{P4.2}$ are obtained by solving the convex SDP problems. According to the above discussions, the objective function in $\mathbf{P1}$ is monotonically non-decreasing after each iteration in Algorithm 3, and Algorithm 3 is guaranteed to converge.

E. Complexity Analysis

To facilitate the computational complexity analysis of the proposed BSS algorithm, we first analyze the computational complexity of each subproblem in one iteration. The TAO subproblem $\mathbf{P2}$ is solved by the CVX toolbox using the interior-point method. According to [11], the computational complexity of the interior-point method is $\mathcal{O}_{\mathrm{TAO}}(T_{\mathrm{dim}}^{3.5}\log(\frac{1}{\epsilon}))$, where T_{dim} denotes the dimension of $\mathbf{P2}$, and ϵ denotes the target accuracy. For the BO subproblem $\mathbf{P3}$, the computational complexity of Algorithm 1 is dominated by solving the SDR problem, i.e., $\mathbf{P3.2}$, according to [38] as

$$\mathcal{O}_{\mathrm{SDR}}(n_{\mathrm{sdp}}^{0.5}(m_{\mathrm{sdp}}n_{\mathrm{sdp}}^3 + m_{\mathrm{sdp}}^2 n_{\mathrm{sdp}}^2 + m_{\mathrm{sdp}}^3)\log(\frac{1}{\epsilon})), \tag{64}$$

where n_{sdp} denotes the dimension of the semi-definite cone constraint, and m_{sdp} denotes the number of semi-definite cone constraint. According to $\mathbf{P3.2}$, we have $n_{\mathrm{sdp}} = MQ$ and $m_{\mathrm{sdp}} = M + 2K + 3$. Besides, the computational complexity of the Gaussian randomization is $\mathcal{O}(VM^2Q^2)$ [39], where V denotes the number of Gaussian randomization samples. Then the computational complexity of Algorithm 1 is $\mathcal{O}_{\mathrm{BO}}(I_{\max}(M^{0.5}Q^{0.5}((M+2K+3)M^3Q^3 + (M+2K+3)^2M^2Q^2 + (M+2K+3)^3)\log(\frac{1}{\epsilon}) + VM^2Q^2))$. For the RCO subproblem $\mathbf{P4}$, the computational complexity of Algorithm 2 is $\mathcal{O}_{\mathrm{RCO}}(I_{\max}((K+1)^{0.5}((3K+3)(K+1)^3 + (3K+3)^2(K+1)^2 + (3K+3)^3)\log(\frac{1}{\epsilon}) + V(K+1)^2))$. According to $\mathcal{O}_{\mathrm{TAO}}$, $\mathcal{O}_{\mathrm{BO}}$, and $\mathcal{O}_{\mathrm{RCO}}$, the computational complexity of BSS Algorithm is $\mathcal{O}_{\mathrm{BSS}}(I_{\max}(\mathcal{O}_{\mathrm{TAO}} + \mathcal{O}_{\mathrm{BO}} + \mathcal{O}_{\mathrm{RCO}}))$.

TABLE II
NUMERICAL PARAMETERS

Descriptions	Parameters and Values
Network model	$K = 4$ [4], $L = 3$ [18], $M = 2$, $Q = 4$ [39]
Channel model	$\gamma = 2.7$, $\sigma^2 = -110$ dBm, $\vartheta = -5$ dB [40]
Transmission model	$T = 1$ s, $\eta = 0.8$, $B = 10$ MHz, $N = 64$ [39], $P_{\mathrm{cir,C}}^B = 200$ μW [41], $P_{\mathrm{cir,P}}^B = 600$ μW [42], $P_{\mathrm{cir}}^A = 1$ mW [41], $P_m = 10$ W, $P_t = 1$ W

V. SIMULATION RESULTS

In the simulations, APs are randomly located in a circle centered at (0, 0) with a radius of 50 m, and BDs are randomly located in a circle centered at (0, 0) with a radius of 5 m. The number of BDs is set as $K = 4$ [4], number of BD's antennas is set as $L = 3$ [18], duration of each time slot is set as $T = 1$ s, path loss exponent is set as $\gamma = 2.7$, power of CSCG noise is set as $\sigma^2 = -110$ dBm, EH efficiency coefficient is set as $\eta = 0.8$, bandwidth is set as $B = 10$ MHz, spreading factor is set as $N = 64$ [39], performance gap between the Shannon capacity and PSK modulation is set as $\vartheta = -5$ dB [40], circuit power for backscatter communication of BDs during the CSR phase is set as $P_{\mathrm{cir,C}}^B = 200$ μW [41], circuit power for backscatter communication of BDs during the PSR phase is set as $P_{\mathrm{cir,P}}^B = 600$ μW [42], and circuit power for AC of BDs during the AC phase is set as $P_{\mathrm{cir}}^A = 1$ mW [41]. Unless otherwise specified, the number of APs is set as $M = 2$, number of AP's antennas is set as $Q = 4$ [39], maximum transmit power of AP_m is set as $P_m = 10$ W, training power P_t is set as 1 W, and total training pilot sequence length is set as $\tau_1 + \tau_2 = 200$. For readability, the key simulation parameters are summarized in Table II, which includes the values and corresponding sources. $\bar{R}_{b,\mathrm{sum}}$ in the CF-SRN and the proposed BSS algorithm, we provide six comparison schemes as follows.

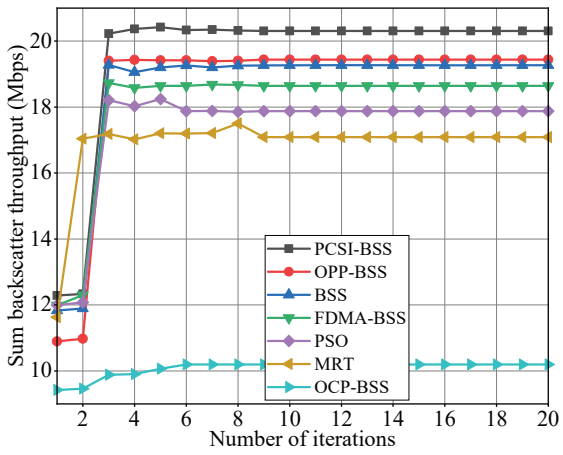

Fig. 4. Sum backscatter throughput $\bar{R}_{b,\text{sum}}$ versus the number of iterations.

- Maximum ratio transmission (MRT) scheme [19]: The beamforming vectors are obtained by MRT. To be specific, the beamforming vectors of APs are aligned with the direct link for primary communication, i.e., $\mathbf{w}_m^X = \sqrt{P_m}\frac{\mathbf{h}_m}{\|\mathbf{h}_m\|}, \forall X \in \{C, P\}$. We adopt MRT to obtain $\{\mathbf{w}^C, \mathbf{w}^P, \mathbf{w}^A\}$, adopt the LP method to obtain $\boldsymbol{t}$, and adopt Algorithm 2 to obtain $\boldsymbol{\alpha}$.
- Particle swarm optimization (PSO) scheme: We adopt PSO to obtain $\boldsymbol{\alpha}$, adopt the LP method to obtain $\boldsymbol{t}$, and adopt Algorithm 1 to obtain $\{\mathbf{w}^C, \mathbf{w}^P, \mathbf{w}^A\}$.
- Frequency division multiple access (FDMA)-BSS scheme: FDMA scheme is adopted by BDs to transmit the environmental data during the AC phase. We adopt the BSS scheme to obtain $\{\mathbf{w}^C, \mathbf{w}^P, \mathbf{w}^A, \boldsymbol{t}, \boldsymbol{\alpha}\}$
- Perfect CSI (PCSI)-BSS scheme: We consider the APs, BDs, and receiver have global perfect CSI, and adopt the proposed BSS scheme to obtain $\{\mathbf{w}^C, \mathbf{w}^P, \mathbf{w}^A, \boldsymbol{t}, \boldsymbol{\alpha}\}$.
- Only CSR phase (OCP)-BSS scheme: Each time slot is divided into the CSR phase and AC phase, and we adopt the proposed BSS scheme to obtain $\{\mathbf{w}^C, \mathbf{w}^P, \mathbf{w}^A, \boldsymbol{t}, \boldsymbol{\alpha}\}$.
- Only PSR phase (OPP)-BSS scheme: Each time slot is divided into the PSR phase and AC phase, and we adopt the proposed BSS scheme to obtain $\{\mathbf{w}^C, \mathbf{w}^P, \mathbf{w}^A, \boldsymbol{t}, \boldsymbol{\alpha}\}$.

As shown in Fig. 4, we plot the sum backscatter throughput $\bar{R}_{b,\text{sum}}$ versus the number of iterations to evaluate the convergence of the proposed BSS algorithm. We observe that the proposed BSS scheme reaches stationary $\bar{R}_{b,\text{sum}}$ within 3 iterations, which verifies the advantage of the BSS scheme in terms of convergence. We also observe that, $\bar{R}_{b,\text{sum}}$ under the proposed BSS scheme is larger than that under the FDMA-BSS scheme. This is due to the reason that, the proposed BSS scheme adopts the uplink NOMA scheme for the BDs to transmit the environmental data during the AC phase, and considers the CSI for dynamically optimizing the beamforming vectors of the BDs to alleviate interference among the BDs, whereas the FDMA-BSS scheme overlooks the CSI and equally allocates spectrum resource to the BDs. We also observe that, $\bar{R}_{b,\text{sum}}$ under the proposed BSS scheme is larger than that under the MRT scheme and PSO scheme, which verifies the superiority of the proposed Algorithm 1 and Algorithm 2 in terms of $\bar{R}_{b,\text{sum}}$. The reason is that, by optimizing the beamforming vectors of the APs, the BSS scheme balances the tradeoff between satisfying the minimum sum primary throughput constraint in (44b) and maximizing $\bar{R}_{b,\text{sum}}$, while the MRT scheme ignores the presence of BDs, and it is easy for the PSO scheme to fall into the local optimal solution of the high-dimensional complex problem [43].

Fig. 5 plots $\bar{R}_{b,\text{sum}}$ versus training power P_t with seven values of total training pilot sequence length $\tau_1 + \tau_2$. We observe that $\bar{R}_{b,\text{sum}}$ increases with P_t. This is due to the reason that, the increase of P_t means that the APs receive stronger pilot signals during CE phase, obtain more accurate estimation channels based on the LMMSE model, and reduce CE errors. More accurate CE facilitates the optimization of beamforming vectors, thereby enhancing $\bar{R}_{b,\text{sum}}$. Smaller CE errors decrease the values of $\mathbb{E}_{\tilde{\mathbf{h}}_m, \tilde{\mathbf{v}}_{m,k}}[\text{ER}^X], \forall X \in \{C, P\}$ in (40), which reduces the interference caused by CE errors and enhances $\bar{R}_{b,\text{sum}}$. We also observe that $\bar{R}_{b,\text{sum}}$ increases with $\tau_1 + \tau_2$. This is due to the reason that, the increase of $\tau_1 + \tau_2$ means that the pilot signals provide more CSI, allowing the APs to perform more accurate CE.

Fig. 6 plots $\bar{R}_{b,\text{sum}}$ under three schemes versus minimum sum primary throughput $R_{\min}$ with two values of P_m, in order to validate the superiority of the proposed hybrid CSR-PSR setup in terms of $\bar{R}_{b,\text{sum}}$. We observe that, the OPP-BSS scheme and proposed BSS scheme achieve similar $\bar{R}_{b,\text{sum}}$. This is due to the reason that, with hybrid CSR-PSR setup, the CF-SRN under the BSS scheme dynamically optimizes the time allocation vector, i.e., the duration of the CSR phase and that of the PSR phase, to balance the tradeoff between satisfying (44b) and maximizing $\bar{R}_{b,\text{sum}}$, which leads to similar $\bar{R}_{b,\text{sum}}$. We also observe that, the CF-SRN under the OPP-BSS scheme with $P_m = 40$ dBm experiences outages when $R_{\min} > 10$ Mbps. This is due to the reason that, there are only PSR phase and AC phase in the OPP-BSS scheme, and primary communication suffers interference from backscatter communication during the PSR phase. When $R_{\min} > 10$ Mbps, the CF-SRN under the OPP-BSS scheme with $P_m = 40$ dBm fails to satisfy (44b). Besides, we also observe that, $\bar{R}_{b,\text{sum}}$ under the OCP-BSS scheme is smallest. This is due to the reason that, there are only CSR phase and AC phase in the OCP-BSS scheme. According to (26) and (33), (3) results in that the BDs under CSR setup achieve lower data rate than that under PSR setup.

Fig. 7 plots the time allocation $\boldsymbol{t}$ under the proposed BSS algorithm with $P_m = 40$ dBm versus $R_{\min}$. We observe that, the duration of the CSR phase t_1 increases with $R_{\min}$. The reason is that, with the increase of $R_{\min}$, the CF-SRN allocates more time to the CSR phase to assist the primary communication. We observe that, the duration of the PSR phase t_2 decreases with $R_{\min}$. The reason is that, the primary communication suffers interference from backscatter communication during the PSR phase. With the increase of $R_{\min}$, the CF-SRN allocates less time to the PSR phase to reduce the interference to the primary communication. We also observe that, the duration of the AC phase t_3 decreases with $R_{\min}$. The reason is that, with the increase of $R_{\min}$, the optimized beamforming vectors of the APs provide more beamforming gains for primary communication to satisfy the minimum sum

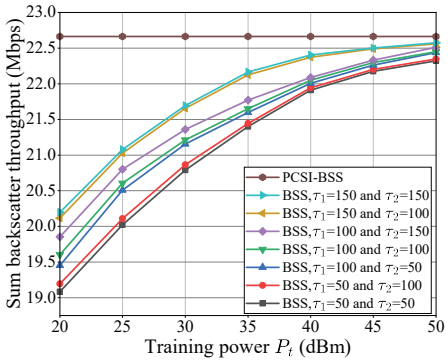

Fig. 5. $\bar{R}_{b,\text{sum}}$ versus training power P_t.

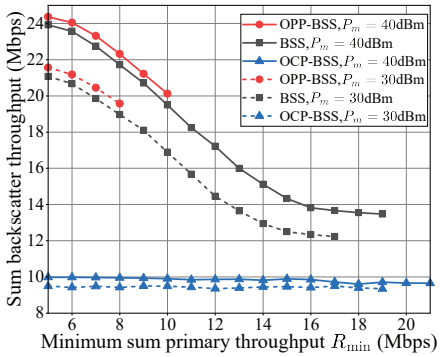

Fig. 6. $\bar{R}_{b,\text{sum}}$ under three schemes versus $R_{\min}$.

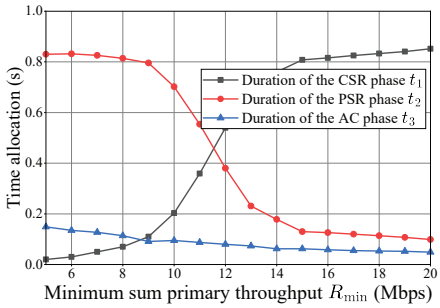

Fig. 7. Time allocation $\boldsymbol{t}$ versus $R_{\min}$.

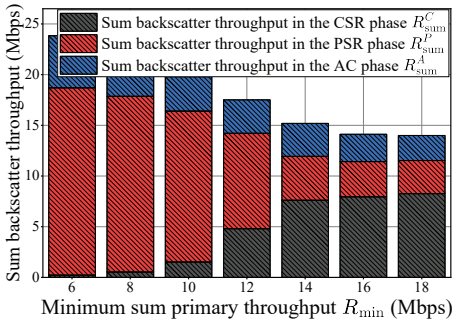

Fig. 8. Backscatter throughput in three phases versus $R_{\min}$.

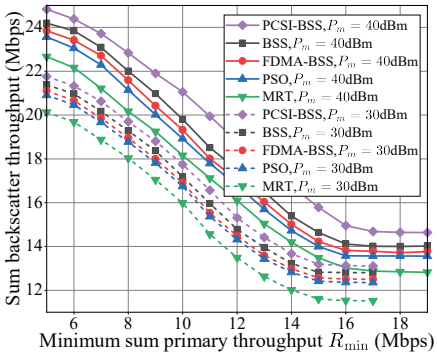

Fig. 9. $\bar{R}_{b,\text{sum}}$ under five schemes versus $R_{\min}$.

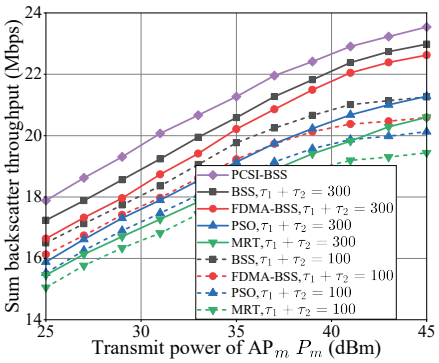

Fig. 10. $\bar{R}_{b,\text{sum}}$ versus P_m.

primary throughput constraint, and reduce the beamforming gains for EH performed by the BDs during the CSR phase and PSR phase, resulting in the decrease of total harvested energy by the BDs. Then the CF-SRN decreases the duration of AC phase due to the limited harvested energy of BDs. Based on the above observations and corresponding reasons, we provide insights as follows: 1) When $R_{\min}$ is small, the CF-SRN allocates more time to the PSR phase and decreases the duration of the CSR phase. When the duration of the CSR phase approaches zero, the hybrid CSR-PSR is reduced to hybrid PSR-AC [9]. 2) When $R_{\min}$ is large, the CF-SRN allocates more time to the CSR phase and decreases the duration of the PSR phase. When duration of the PSR phase approaches zero, the hybrid CSR-PSR is reduced to hybrid CSR-AC [5].

Fig. 8 plots the backscatter throughput in three phases under the proposed BSS algorithm with $P_m = 40$ dBm versus $R_{\min}$. We observe that, the backscatter throughput during the PSR phase R^P_{sum} decreases with $R_{\min}$. The reason is that, with the increase of $R_{\min}$, the duration of the PSR phase t_2 decreases to reduce the interference to the primary communication. We observe that, the backscatter throughput during the CSR phase R^C_{sum} increases with $R_{\min}$. The reason is that, the duration of the CSR phase t_1 increases with $R_{\min}$ in order to satisfy the minimum sum primary throughput constraint. We also observe that, the throughput of BDs during the AC phase R^A_{sum} decreases with $R_{\min}$. The reason is that, with the increase of $R_{\min}$, the CF-SRN allocates less time to the AC phase due to the decreased harvested energy of BDs.

Fig. 9 plots $\bar{R}_{b,\text{sum}}$ under five schemes versus $R_{\min}$ with two values of P_m. We observe that $\bar{R}_{b,\text{sum}}$ decreases with $R_{\min}$. The reason is that, with the increase of $R_{\min}$, the optimized beamforming vectors of the APs provide more beamforming gains for primary communication to satisfy (44b), while diminishing the gains for backscatter communication. We also observe that five schemes with $P_m = 30$ dBm experience outages when $R_{\min} > 17$ Mbps. The reason is that, when P_m is small, the CF-SRN under five schemes with limited power budget fails to obtain a feasible solution of $\mathbf{P1}$. Besides, we also observe that $\bar{R}_{b,\text{sum}}$ under five schemes with $P_m = 40$ dBm remain almost unchanged when $R_{\min} > 16$ Mbps. The reason is that, when $R_{\min}$ is large, the CF-SRN under hybrid CSR-PSR setup decreases the duration of PSR phase and increases that of CSR phase to satisfy (44b), and the duration of the time slot is dominated by CSR phase. Based on (3), the backscatter symbols transmitted by BDs during CSR phase are less than those during PSR phase, backscatter communication in CSR phase occupies less beamforming resource for transmitting backscatter symbols, and $R_{\min}$ has smaller impact on $\bar{R}_{b,\text{sum}}$ with the decrease of the PSR phase duration.

Fig. 10 plots $\bar{R}_{b,\text{sum}}$ versus P_m with two values of $\tau_1 + \tau_2$. We observe that, $\bar{R}_{b,\text{sum}}$ increases with P_m. This observation is due to two reasons. 1) According to (19) and (27), the increase of P_m means that, the APs transmit stronger RF signals, enhancing the symbiotic relationship between the APs and BDs, and facilitating the backscatter communication for

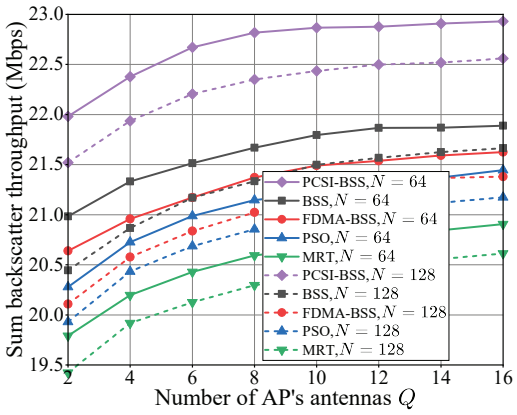

Fig. 11. $\bar{R}_{b,\text{sum}}$ versus number of AP's antennas Q.

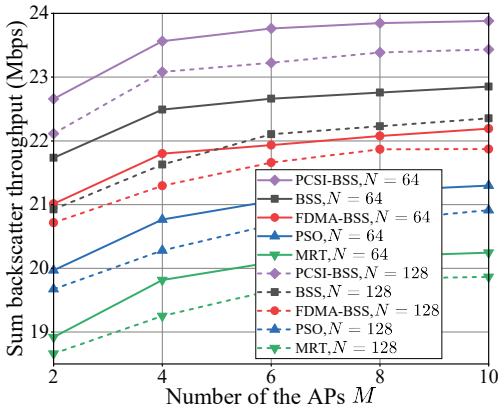

Fig. 12. $\bar{R}_{b,\text{sum}}$ versus number of the APs M.

increasing $\bar{R}_{b,\text{sum}}$. 2) According to (7) and (10), E_k^{total} in (11) increases with P_m, which allows BD_k to consume more energy for AC during the AC phase, resulting in the increase of $\bar{R}_{b,\text{sum}}$ according to (13) and (36).

Figs. 11 and 12 plot $\bar{R}_{b,\text{sum}}$ versus the number of AP's antennas Q and that of the APs M with two values of N. We observe that $\bar{R}_{b,\text{sum}}$ increases with Q and M, respectively. This is due to the reason that, the increase of Q means that the APs exploit more spatial diversity, and provide more beamforming gains for the BDs to perform backscatter communication and EH, resulting in the increase of $\bar{R}_{b,\text{sum}}$. The increase of M means that more APs cooperatively transmit primary RF signals to the receiver, and provide more beamforming gains for the BDs. We also observe that, $\bar{R}_{b,\text{sum}}$ with $N = 64$ is larger than that with $N = 128$, which is due to the mathematical relationship between N and $\bar{R}_{b,\text{sum}}$ in (42).

VI. Conclusion

In the CF-SRN with hybrid CSR-PSR setup, we formulated the sum backscatter throughput maximization problem by jointly optimizing the time allocation vector, beamforming vectors of the APs and BDs, and reflection coefficients of the BDs. To tackle the coupled relationship among high-dimensional variables, we decomposed the formulated problem into three subproblems, and solved the three subproblems alternately under the proposed BSS algorithm. Through simulation results, we summarized the main findings as follows: 1) For the sum backscatter throughput maximization problem with multiple coupled reflection coefficient variables, the approximate optimal solution can be obtained through the matrix transformation, SDR method, and SCA method. 2) The hybrid CSR-PSR setup outperforms the CSR setup in terms of $\bar{R}_{b,\text{sum}}$, and outperforms the PSR setup in terms of $R_{\min}$. We provided insights as follows: 1) The PSR phase is beneficial for the CF-SRN to achieve the sum backscatter throughput. When $R_{\min}$ is small, the CF-SRN increases the duration of the PSR phase to maximize the sum backscatter throughput. 2) The CSR phase is beneficial for the CF-SRN to achieve the sum primary throughput. When $R_{\min}$ is large, the CF-SRN increases the duration of the CSR phase to satisfy the minimum sum primary throughput constraint. Future works include the PSK phase optimization, inter-receiver interference management in the multi-receiver scenario, and comparison between the CF-SRN and cellular SRN.

Appendix A
Proof of Lemma 1

We calculate $\mathbb{E}_{\tilde{\mathbf{h}}_m,\tilde{\mathbf{v}}_{m,k}}[\text{ER}^C]$ as

$$\begin{aligned}
&\mathbb{E}_{\tilde{\mathbf{h}}_m,\tilde{\mathbf{v}}_{m,k}}[\text{ER}^C]\\
=&\mathbb{E}_{\tilde{\mathbf{h}}_m,\tilde{\mathbf{v}}_{m,k}}\left[\left|\sum_{m=1}^{M}\left(\tilde{\mathbf{h}}_m+\sum_{k=1}^{K}\sqrt{\alpha_k}\tilde{\mathbf{v}}_{m,k}\right)^{\text{H}}\mathbf{w}_m^C\right|^2\right]\\
\overset{(a)}{=}&\mathbb{E}_{\tilde{\mathbf{h}}_m,\tilde{\mathbf{v}}_{m,k}}\Bigg[\sum_{m=1}^{M}\sum_{l=1}^{M}(\mathbf{w}_m^C)^{\text{H}}\Big(\tilde{\mathbf{h}}_m\tilde{\mathbf{h}}_l^{\text{H}}+\sum_{i=1}^{K}\sqrt{\alpha_i}\tilde{\mathbf{h}}_m\tilde{\mathbf{v}}_{l,i}^{\text{H}}\\
&+\sum_{k=1}^{K}\sqrt{\alpha_k}\tilde{\mathbf{v}}_{m,k}\tilde{\mathbf{h}}_l^{\text{H}}+\sum_{k=1}^{K}\sum_{i=1}^{K}\sqrt{\alpha_k}\sqrt{\alpha_i}\tilde{\mathbf{v}}_{m,k}\tilde{\mathbf{v}}_{l,i}\Big)\mathbf{w}_l^C\Bigg]\\
\overset{(b)}{=}&\sum_{m=1}^{M}(\mathbf{w}_m^C)^{\text{H}}\Big(\mathbb{E}\left[\tilde{\mathbf{h}}_m\tilde{\mathbf{h}}_m^{\text{H}}\right]+\sum_{k=1}^{K}\alpha_k c_k^2\mathbb{E}\left[\tilde{\mathbf{v}}_{m,k}\tilde{\mathbf{v}}_{m,k}^{\text{H}}\right]\Big)\mathbf{w}_m^C\\
\overset{(c)}{=}&\sum_{m=1}^{M}(\mathbf{w}_m^C)^{\text{H}}\Big(\mathbf{C}_m+\sum_{k=1}^{K}\alpha_k\mathbf{C}_{m,k}\Big)\mathbf{w}_m^C,
\end{aligned}\tag{65}$$

where (a) follows the fact that given $\mathbf{a}\in\mathbb{C}^{J\times 1}$, $|\mathbf{a}|^2=\mathbf{a}^{\text{H}}\mathbf{a}$ holds. Specifically, $J=1$ in (a) holds. For $m\in\mathcal{M}$ and $k\in\mathcal{K}$, (b) in (65) follows the fact that $\tilde{\mathbf{h}}_m$ and $\tilde{\mathbf{v}}_{m,k}$ are independent, and both $\tilde{\mathbf{h}}_m$ and $\tilde{\mathbf{v}}_{m,k}$ are i.i.d. random variables. Then we have $\mathbb{E}[\tilde{\mathbf{h}}_m\tilde{\mathbf{v}}_{m,k}]=0$, $\mathbb{E}[\tilde{\mathbf{h}}_m\tilde{\mathbf{h}}_l]=0$ $(m\neq l)$, and $\mathbb{E}[\tilde{\mathbf{v}}_{m,k}\tilde{\mathbf{v}}_{l,i}]=0$ $(m\neq l$ or $k\neq i)$. (c) in (65) follows the fact that $\tilde{\mathbf{h}}_m\sim\mathcal{CN}(0,\mathbf{C}_m)$ and $\tilde{\mathbf{v}}_{m,k}\sim\mathcal{CN}(0,\mathbf{C}_{m,k})$. Then we have $\mathbb{E}[\tilde{\mathbf{h}}_m\tilde{\mathbf{h}}_m^{\text{H}}]=\mathbf{C}_m$ and $\mathbb{E}[\tilde{\mathbf{v}}_{m,k}\tilde{\mathbf{v}}_{m,k}^{\text{H}}]=\mathbf{C}_{m,k}$.

Similar to (65), we calculate $\mathbb{E}_{\tilde{\mathbf{h}}_m,\tilde{\mathbf{v}}_{m,k}}[\text{ER}^P]$ as

$$\mathbb{E}_{\tilde{\mathbf{h}}_m,\tilde{\mathbf{v}}_{m,k}}[\text{ER}^P]=\sum_{m=1}^{M}(\mathbf{w}_m^P)^{\text{H}}\Big(\mathbf{C}_m+\sum_{k=1}^{K}\alpha_k\mathbf{C}_{m,k}\Big)\mathbf{w}_m^P.\tag{66}$$

References

[1] X. Liu, J. Xu, K. Zheng, G. Zhang, J. Liu, and N. Shiratori, "Throughput maximization with an AoI constraint in energy harvesting D2D-enabled cellular networks: An MSRA-TD3 approach," *IEEE Trans. Wireless Commun.*, vol. 24, no. 2, pp. 1448–1466, Feb. 2025.

[2] Q. Sun, Y. Zhou, Y. Shen, F. Li, X. Chen, D. Li, and J. Zhang, "Uplink performance of cell-free symbiotic radio with hardware impairments for IoT," *IEEE Internet Things J.*, vol. 12, no. 13, pp. 23418–23433, Mar. 2025.

[3] D. Jia, F. Hu, Z. Ling, H. Li, and Y. Gao, "Computation offloading and resource allocation in symbiotic radio-assisted HSR networks: A fingerprint-based distributed D3QN approach," *IEEE Trans. Commun.*, vol. 73, no. 11, pp. 11528–11544, Jun. 2025.

[4] J. Wang, Y.-C. Liang, and S. Sun, "Multi-user multi-IoT-device symbiotic radio: A novel massive access scheme for cellular IoT," *IEEE Trans. Wireless Commun.*, vol. 23, no. 9, pp. 11876–11889, Sep. 2024.

[5] R. Xu, Y. Ye, H. Sun, L. Shi, and G. Lu, "Revolutionizing symbiotic radio: Exploiting trade-offs in hybrid active-passive communications," *IEEE Commun. Mag.*, vol. 63, no. 9, pp. 156–163, Jun. 2025.

[6] R. Long, Y.-C. Liang, H. Guo, G. Yang, and R. Zhang, "Symbiotic radio: A new communication paradigm for passive Internet of Things," *IEEE Internet Things J.*, vol. 7, no. 2, pp. 1350–1363, Feb. 2020.

[7] X. Liu, H. Zhang, K. Bian, X. Weng, and L. Song, "Meta-backscatter: A new ISAC paradigm for battery-free internet of things," *IEEE Commun. Mag.*, vol. 62, no. 9, pp. 106–112, Sep. 2024.

[8] Y. Xu, X. Zuo, G. Yang, X. Li, S. Gong, C. Huang, and C. Yuen, "Outage-constrained throughput maximization for MISO symbiotic radio systems," *IEEE Trans. Veh. Technol.*, vol. 73, no. 11, pp. 16725–16734, Nov. 2024.

[9] Y. Zhuang, X. Li, H. Ji, H. Zhang, and V. C. M. Leung, "Optimal resource allocation for RF-powered underlay cognitive radio networks with ambient backscatter communication," *IEEE Trans. Veh. Technol.*, vol. 69, no. 12, pp. 15216–15228, Nov. 2020.

[10] L. Shi, Y. Ye, X. Chu, G. Lu, and S. Sun, "Resource allocation for multi-IoT-node mutualistic symbiotic radio with hybrid long and short packets," *IEEE Trans. Wireless Commun.*, early access, Aug. 15, 2025, doi: 10.1109/TWC.2025.3593290.

[11] J. Xu, Z. Dai, and Y. Zeng, "MIMO symbiotic radio with massive backscatter devices: Asymptotic analysis and precoding optimization," *IEEE Trans. Commun.*, vol. 71, no. 9, pp. 5487–5502, Sep. 2023.

[12] C. Zhou, B. Lyu, C. You, and D. T. Hoang, "Cooperative commensal and parasitic symbiotic radio communication systems," *IEEE Wireless Commun. Lett.*, vol. 13, no. 3, pp. 676–680, Mar. 2024.

[13] Y. Zhang, B. Di, H. Zhang, J. Lin, C. Xu, D. Zhang, Y. Li, and L. Song, "Beyond cell-free MIMO: Energy efficient reconfigurable intelligent surface aided cell-free MIMO communications," *IEEE Trans. Cognit. Commun. Networking*, vol. 7, no. 2, pp. 412–426, Jun. 2021.

[14] H. Q. Ngo, A. Ashikhmin, H. Yang, E. G. Larsson, and T. L. Marzetta, "Cell-free massive MIMO versus small cells," *IEEE Trans. Wireless Commun.*, vol. 16, no. 3, pp. 1834–1850, Mar. 2017.

[15] G. R. Gopal and B. D. Rao, "Vector quantization methods for access point placement in cell-free massive MIMO systems," *IEEE Trans. Wireless Commun.*, vol. 23, no. 6, pp. 5425–5440, Jun. 2024.

[16] M. Jadidi, A. M. Khoueini, A. Mohammadi, and V. Meghdadi, "Performance analysis and power allocation for uplink cell-free massive MIMO system with nonlinear power amplifier," *IEEE Trans. Commun.*, vol. 72, no. 9, pp. 5473–5485, Sep. 2024.

[17] Y. Hu, J. Zhang, E. Shi, Y. Lu, J. An, C. Yuen, and B. Ai, "Joint beamforming and power allocation design for stacked intelligent metasurfaces-aided cell-free massive MIMO systems," *IEEE Trans. Veh. Technol.*, vol. 74, no. 3, pp. 5235–5240, Mar. 2025.

[18] Z. Dai, R. Li, J. Xu, Y. Zeng, and S. Jin, "Rate-region characterization and channel estimation for cell-free symbiotic radio communications," *IEEE Trans. Commun.*, vol. 71, no. 2, pp. 674–687, Feb. 2023.

[19] F. Li, Q. Sun, X. Chen, and J. Zhang, "Spectral efficiency analysis of uplink cell-free massive MIMO symbiotic radio," *IEEE Internet Things J.*, vol. 11, no. 2, pp. 3614–3627, Jul. 2024.

[20] B. Lyu, C. Zhou, S. Gong, W. Wu, D. T. Hoang, and D. Niyato, "Energy-efficiency maximization for STAR-RIS enabled cell-free symbiotic radio communications," *IEEE Trans. Cognit. Commun. Networking*, vol. 10, no. 6, pp. 2209–2223, May 2024.

[21] Z. Dai, J. Xu, Y. Zeng, S. Jin, and T. Jiang, "Characterizing the rate region of active and passive communications with RIS-based cell-free symbiotic radio," *IEEE Internet Things J.*, vol. 11, no. 4, pp. 5653–5666, Feb. 2024.

[22] F. Li, Q. Sun, X. Chen, S. Dang, J. Zhang, and K.-K. Wong, "Rate-splitting assisted cell-free symbiotic radio: Channel estimation and transmission scheme," *IEEE Trans. Commun.*, vol. 73, no. 7, pp. 5313–5327, Dec. 2025.

[23] L. Li, X. Huang, and Y. Fang, "Hierarchical multiple access for spectrum-energy opportunistic ambient backscatter wireless networks," *IEEE Trans. Mobile Comput.*, vol. 22, no. 8, pp. 4648–4663, Aug. 2023.

[24] Z. Ling, F. Hu, H. Zhang, and Z. Han, "Age-of-information minimization in healthcare IoT using distributionally robust optimization," *IEEE Internet Things J.*, vol. 9, no. 17, pp. 16154–16167, Feb. 2022.

[25] F. Zhu, M. Ouyang, L. Feng, Y. Liu, X. Tian, M. Jin, D. Chen, and X. Wang, "Enabling software-defined PHY for backscatter networks," in *Proc. 20th Annu. Int. Conf. Mobile Syst. Appl. Serv.*, 2022, pp. 330–342.

[26] Y. Ye, S. Lu, L. Shi, X. Chu, and S. Sun, "Symbiotic backscatter communication: A design perspective on the modulation scheme of backscatter devices," 2025, *arXiv:2507.01782*. [Online]. Available: https://arxiv.org/abs/2507.01782

[27] D. Jia, F. Hu, Q. Zhang, Z. Ling, and Y.-C. Liang, "Distributed deep reinforcement learning-based power control and device access for high-speed railway networks with symbiotic radios," *IEEE Trans. Commun.*, vol. 73, no. 2, pp. 1201–1216, Aug. 2025.

[28] R. Du, T. O. Timoudas, and C. Fischione, "Comparing backscatter communication and energy harvesting in massive IoT networks," *IEEE Trans. Wireless Commun.*, vol. 21, no. 1, pp. 429–443, Jan. 2022.

[29] Y. Yuan, S. Wang, Y. Wu, H. V. Poor, Z. Ding, X. You, and L. Hanzo, "NOMA for next-generation massive IoT: Performance potential and technology directions," *IEEE Commun. Mag*, vol. 59, no. 7, pp. 115–121, Jul. 2021.

[30] A. Ihsan, W. Chen, S. Zhang, and S. Xu, "Energy-efficient NOMA multicasting system for beyond 5G cellular V2X communications with imperfect CSI," *IEEE Trans. Intell. Transp. Syst.*, vol. 23, no. 8, pp. 10721–10735, Aug. 2022.

[31] Q. Zhang, Y.-C. Liang, H.-C. Yang, and H. V. Poor, "Mutualistic mechanism in symbiotic radios: When can the primary and secondary transmissions be mutually beneficial?," *IEEE Trans. Wireless Commun.*, vol. 21, no. 10, pp. 8036–8050, Oct. 2022.

[32] Z. Tu, R. Long, Y. Pei, and Y.-C. Liang, "RIS-enabled full-duplex backscatter communication in multi-user symbiotic radio," *IEEE Trans. Wireless Commun.*, vol. 23, no. 11, pp. 16261–16274, Nov. 2024.

[33] Y. Ye, L. Shi, X. Chu, and G. Lu, "Total transmission time minimization in wireless powered hybrid passive-active communications," in *Proc. IEEE 93rd Veh. Technol. Conf. (VTC),* Helsinki, Finland, Apr. 2021, pp. 1–5.

[34] Y. Xu, M. Wang, H. Zhang, Q. Xue, J. Kang, Q. Chen, and C. Yuen, "Resource allocation for RSMA-based symbiotic radio systems under imperfect SIC and CSI," *IEEE Trans. Veh. Technol.*, vol. 74, no. 3, pp. 5170–5174, Mar. 2025.

[35] Z.-Q. Luo, W.-K. Ma, A. M.-C. So, Y. Ye, and S. Zhang, "Semidefinite relaxation of quadratic optimization problems," *IEEE Signal Process. Mag.*, vol. 27, no. 3, pp. 20–34, May 2010.

[36] Y. Li, J. Wang, Y. Zou, W. Xie, and Y. Liu, "Weighted sum power maximization for STAR-RIS assisted SWIPT systems," *IEEE Trans. Wireless Commun.*, vol. 23, no. 12, pp. 18394–18408, Dec. 2024.

[37] L. Zhao, H. Xu, S. Qu, Z. Wei, and Y. Liu, "Joint trajectory and communication design for UAV-assisted symbiotic radio networks," *IEEE Trans. Veh. Technol.*, vol. 73, no. 6, pp. 8367–8378, Jan. 2024.

[38] H. Fu, S. Feng, W. Tang, and D. W. K. Ng, "Robust secure beamforming design for two-user downlink MISO rate-splitting systems," *IEEE Trans. Wireless Commun.*, vol. 19, no. 12, pp. 8351–8365, Dec. 2020.

[39] X. Xu, Y.-C. Liang, G. Yang, and L. Zhao, "Reconfigurable intelligent surface empowered symbiotic radio over broadcasting signals," *IEEE Trans. Commun.*, vol. 69, no. 10, pp. 7003–7016, Oct. 2021.

[40] D. Li, "Backscatter communication via harvest-then-transmit relaying," *IEEE Trans. Veh. Technol.*, vol. 69, no. 6, pp. 6843–6847, Apr. 2020.

[41] H. Yang, Y. Ye, X. Chu, and S. Sun, "Energy efficiency maximization for UAV-enabled hybrid backscatter-harvest-then-transmit communications," *IEEE Trans. Wireless Commun.*, vol. 21, no. 5, pp. 2876–2891, Oct. 2022.

[42] J. D. Rosenthal and M. S. Reynolds, "Hardware-efficient all-digital architectures for OFDM backscatter modulators," *IEEE Trans. Microwave Theory Tech.*, vol. 69, no. 1, pp. 803–811, Dec. 2021.

[43] Z. Zhao, H. Cheng, X. Xu, and Y. Pan, "Graph partition and multiple choice-UCB based algorithms for edge server placement in MEC environment," *IEEE Trans. Mobile Comput.*, vol. 23, no. 5, pp. 4050–4061, May 2024.

Kechen Zheng (Senior Member, IEEE) received the B.E. and Ph.D. degrees in electronic engineering from Shanghai Jiao Tong University, Shanghai, China, in 2013 and 2018, respectively. He is currently an Associate Professor with the School of Computer Science and Technology, Zhejiang University of Technology, Hangzhou, China. He has published more than 50 technical papers in journals and conferences, including IEEE Transactions on Mobile Computing, IEEE Transactions on Wireless Communications, and IEEE Transactions on Communications. His research interests include symbiotic radio, energy harvesting, wireless communication, and edge computing. Dr. Zheng was the recipient of the Best Paper Award at the International Conference on Networking and Network Applications in 2021.

Zefu Li received the B.E. degree from Zhengzhou University of Technology, Zhengzhou, China, in 2023. He is currently pursuing the M.E. degree in computer technology from Zhejiang University of Technology. His current research interests include symbiotic radio and backscatter communication.

Xiaoying Liu (Senior Member, IEEE) received the B.E. degree in electronic engineering from the Nanjing University of Science and Technology, Nanjing, China, in 2013 and the Ph.D. degree in electronic engineering from Shanghai Jiao Tong University, Shanghai, China, in 2018. She is currently an Associate Professor with the School of Computer Science and Technology, Zhejiang University of Technology, Hangzhou, China. Her research interests include cognitive radio, energy-efficient wireless communications, mobile computing, and the Internet of Things. Dr. Liu was the recipient (as the corresponding author) of the Best Paper Award at the International Conference on Networking and Network Applications in 2021.

Jia Liu (Senior Member, IEEE) received the B.E. degree from the School of Telecommunications Engineering, Xidian University, Xi'an, China, in 2010, and the Ph.D. degree from the School of Systems Information Science, Future University Hakodate, Japan, in 2016. His research interests include wireless systems security, space-air-ground integrated networks, the Internet of Things, and 6G. He received the 2016 and 2020 IEEE Sapporo Section Encouragement Award.

Tarik Taleb (Senior Member, IEEE) received the B.E. degree (with distinction) in information engineering, and the M.Sc. and Ph.D. degrees in information sciences from Tohoku University, Sendai, Japan, in 2001, 2003, and 2005, respectively. He is currently a full professor with Ruhr University Bochum, Germany. He was a professor with the Center of Wireless Communications, University of Oulu, Oulu, Finland. He is the founder of ICTFICIAL Oy, and the founder and the director with the MOSA!C Lab, Espoo, Finland. From October 2014 to December 2021, he was an associate professor with the School of Electrical Engineering, Aalto University, Espoo, Finland. Prior to that, he was working as a senior researcher and a 3GPP standards expert with NEC Europe Ltd., Heidelberg, Germany. Before joining NEC and till March 2009, he worked as assistant professor with the Graduate School of Information Sciences, Tohoku University, in a lab fully funded by KDDI. From 2005 to 2006, he was a research fellow with the Intelligent Cosmos Research Institute, Sendai. He has been directly engaged in the development and standardization of the Evolved Packet System as a member of the 3GPP System Architecture Working Group. His current research interests include AI-based network management, architectural enhancements to mobile core networks, network softwarization and slicing, mobile cloud networking, network function virtualization, software-defined networking, software-defined security, and mobile multimedia streaming.

Norio Shiratori (Life Fellow, IEEE) received the Ph.D. degree from Tohoku University in 1977. Since 2017, he has been a Professor with the Research and Development Initiative, Chuo University. He has published over 15 books and over 600 refereed articles in computer science and related fields. He is a fellow of Japan Foundation of Engineering Societies (JFES), the Information Processing Society of Japan (IPSJ), and the Institute of Electronics, Information and Communication Engineers (IEICE). Recognizing his significant contributions, he was honored with the title of IEEE Life Fellow in 2017. He was a recipient of the Minister of MEXT Award from Japanese Government in 2016; the Science and Technology Award from the Ministry of Education, Culture, Sports, Science, and Technology (MEXT), in 2009; the IEICE Achievement Award in 2001; the IEICE Contribution Award in 2011; the IPSJ Contribution Award in 2008; and the IEICE Honorary Member in 2012.